https://doi.org/10.5194/egusphere-2026-4902
Preprint. Discussion started: 27 August 2026

Accounting for shelf-width in selecting altimetry observations for estimating coastal sea level changes improves its agreement with tide gauges

Vandana Sukumaran[1] and Bramha Dutt Vishwakarma[1,2]

[1]Interdisciplinary Centre for Water Research, Indian Institute of Science, Bangalore – 560012, India
[2]Centre for Earth Sciences, Indian Institute of Science, Bangalore – 560012, India

Correspondence to: Vandana Sukumaran (vandanas1@iisc.ac.in)

Abstract. Monitoring coastal sea level change is critical as sea level rise becomes inevitable due to climate change. The global tide gauge (TG) network is sparse and suffers from data gaps, while satellite altimetry performance near the coast remains spatially inconsistent. Here, a novel dynamically varying search radius algorithm (DSR algorithm) is developed that uses bathymetry to choose satellite observations that represent coastal sea level variability better. The DSR algorithm is applied to the low-resolution (1 Hz) coastal product, X-TRACK SLA L2P v2.2 (XTRACK), and is evaluated through comparison with TG and the high-resolution (20 Hz) coastal product, XTRACK/ALES (Along-track sea level anomalies and trends v3.0). To assess the benefit of DSR, existing observation-selection algorithms are applied to both XTRACK and XTRACK/ALES and compared against TG using detrended deseasonalized coastal sea level anomalies. This inter-algorithm comparison at 272 TG stations demonstrates broader applicability of DSR across various coastal regimes, with consistently higher median correlation and lower median Normalized Root Mean Square Error. The improvement using DSR is especially pronounced along narrow coastal shelf regions. Additionally, the DSR-applied XTRACK's ability to capture coastal sea level anomalies at multiple temporal scales is assessed at 264 stations, showing improved agreement for both seasonal (annual) and non-linear trend (interannual and trend) signals. In some regions, such as the eastern Australian coast and Gulf of St. Lawrence, lower correlation and higher Root Mean Square Error for residual signals are reported, which are discussed. Further, Coastal Sea Level Trends (CSLT) for 1994–2023 (30 years) from DSR-based XTRACK match TG trends within their uncertainties. Notably high CSLT values are observed in the Gulf of Mexico (5.09±0.57 mm/yr from altimetry and 5.2±0.67 mm/yr from TG) and the Baltic Sea (4.62±1.3 mm/yr from altimetry and 4.24 ±1.37 mm/yr from TG).

1 Introduction

Sea level rise will be one of the most disastrous consequences of anthropogenic climate change. About 40% of the world's population (~2.5 billion people) lives within 100 km of the coast and would be severely affected (Hauer et al., 2020; Heger and Vashold, 2021; Kummu et al., 2016). Hence, monitoring and understanding coastal sea level change is crucial. Coastal sea level variability differs from open ocean due to the influence of continental slope, shallow waters, fresh water inflow,

https://doi.org/10.5194/egusphere-2026-4902
Preprint. Discussion started: 27 August 2026

vertical land motion (VLM), glacial isostatic adjustment (GIA) and presence of coastlines (Hughes et al., 2018, 2019; Melet et al., 2020; Oelsmann et al., 2024; Swallow, 1963; Woodworth et al., 2019). Tide gauges (TG), the oldest and the direct source of coastal sea level data, are sparse, unevenly distributed, and suffer from data gaps (Emery and Aubrey, 2012; Woodworth et al., 2016). Satellite altimetry has monitored global sea level since 1992, but its reliability near the coast remains limited (Fu and Cazenave, 2000). Closer to the coast, altimetry signals are affected by bright land returns (Qin et al., 2023; Vignudelli et al., 2011a), off-nadir returns from calm water (Dieng et al., 2021; Qin et al., 2023; Vignudelli et al., 2011a), steep waves (Gómez-Enri et al., 2010; Wang and Huang, 2021), and short-scale variability of surface characteristics (Deng and Featherstone, 2006; Qin et al., 2023; Vignudelli et al., 2011a). Off-nadir returns from calm-water contaminate the waveform (Deng and Featherstone, 2006; Gómez-Enri et al., 2010; Violante-Carvalho et al., 2021), while bottom friction in shallow waters produce steep waves which cause a negative bias in significant wave height (SWH) when compared with buoys (Durrant et al., 2009). Small-scale waves reduce nadir backscatter (Gómez-Enri et al., 2010), and short-scale water vapor variations affect the wet-tropospheric correction (Vignudelli et al., 2019). Hence, observations closer than 50km to the coast were neglected until 2010 (Ponte et al., 2020; Vignudelli et al., 2011b).

Several efforts have been made to retrieve coastal sea level signals from different altimetry missions: PISTACH for Jason (2007–2011) (Mercier et al., 2008), COASTALT for Envisat (2008–2012) (Vignudelli et al., 2009), X-TRACK (Birol et al., 2017), PEACHI for AltiKa (Valladeau et al., 2015), ALES (Passaro et al., 2014), SAMOSA+ and SAMOSA++ for SAR altimeters (Dinardo et al., 2018, 2021). Recently, fully focused SAR (FF-SAR) processing has been found to yield sub-meter along-track resolution and more accurate geophysical estimates (like sea surface height (SSH) and SWH) since it is less affected by strongly reflective targets near the coast (Schlembach et al., 2023).

X-TRACK is a dedicated post-processing system for coastal zones that enhances both the quantity and quality of SSH observations (Birol et al., 2017). ALES (Adaptive Leading Edge Subwaveform) retracker derives SSH from coastal and open ocean observations by improving the range term (Passaro et al., 2014). The ALES algorithm has been extensively validated in numerous studies (Gomez-Enri et al., 2016; Passaro et al., 2014, 2015). For example, Marti et al. (2021) used Jason-1 and Jason-2 altimetry data (ALES retracked and X-TRACK post-processed) along the western African coast, using the along-track pass closest to the shoreline, and found coastal sea level trends (CSLT) stable between 15–5 km offshore but varying nearshore. Similarly, Gouzenes et al. (2020) reported good agreement of CSLT beyond 4 km along the coast of Senetosa. Abele et al. (2023) evaluated the performance of ALES and SAMOSA++ using sea level variance in the coastal zone of the northwest Atlantic and found that SAMOSA++ outperformed ALES in the coastal strip less than 10 km from the shore.

Altimetry and TG observations are not co-located and thus, several methods have been used to aggregate altimetry data prior to validation (Dieng et al., 2021; Oelsmann et al., 2021; Vignudelli et al., 2005; Vinogradov and Ponte, 2010). Vinogradov and Ponte (2010) compared annual amplitudes and phases at 345 continental and island stations with altimetry, from TOPEX/Poseidon, using a search radius (SR) of 134 km centered on TG. They found that the correlations of annual amplitudes decrease with increasing depth, and an average correlation of 0.85 in nearby shallow regions. In a separate study, they

https://doi.org/10.5194/egusphere-2026-4902
Preprint. Discussion started: 27 August 2026

compared the low-frequency coastal sea level anomaly (SLA) variability using an SR of 180 km. They reported the best agreement for Pacific and Indian Ocean islands, and western Australia, but observed large discrepancies (> 4 cm Root Mean Square Error) along southwest America, Japan, and eastern Australia (Vinogradov and Ponte, 2011). Birol et al. (2021) compared a new high-resolution coastal altimetry product called XTRACK/ALES (20Hz) with XTRACK (1 Hz and 20 Hz) across several regions (except northwest and northeast America, south America, and eastern Africa). The product uses Jason-1, Jason-2 and Jason-3 measurements retracked with ALES and post-processed with X-TRACK software. They compared the nearest altimetry point (having 80% time-series completeness) with TG, and found that XTRACK/ALES, after filtering, shows slightly higher correlation ($r \geq 0.7$) and better Root Mean Square Error (RMSE) than XTRACK 1 Hz at all stations except Sete. Cazenave et al. (2022) validated monthly SLA from point-level XTRACK/ALES observations and found an average correlation of 0.5, which improved to 0.78 when altimetry was averaged along and across tracks near each TG, due to reduced sampling errors and influence of small-scale variability. Additionally, linear trends also agreed statistically at 64% of stations.

Overall, existing studies are either regional or concerned with certain temporal scales (interannual, annual, trend, residual) and do not compare across various altimetry observation-selection choices. They also indicate a spatial inconsistency in validation results, which means, while satellite altimetry can serve as a reliable proxy for TG in some regions, it struggles to capture coastal sea level variability in others. Therefore, a comprehensive global assessment of coastal altimetry at various temporal scales is needed. Further, existing coastal altimetry processing choices focus on higher quality data obtained closer to the coast for developing coastal sea level products. Since, the coastal sea level variability is more sensitive to local ocean dynamics, which is influenced by the continental shelf-width (Camargo et al., 2024; Huthnance, 1978; Woodworth et al., 2019), we hypothesize that selecting altimetry points along the coast and within the shelf would represent the coastal sea level better. Hence, we develop a novel Dynamic Search Radius (DSR) algorithm, which selects altimetry observations along the coast but within the shelf-break, and apply it on the low-resolution (1 Hz) coastal altimetry product, X-TRACK SLA L2P v2.2 (hereinafter XTRACK). An exhaustive validation and assessment of the DSR algorithm is performed against TG, and a high-resolution (20 Hz) coastal altimetry product (Along-track sea level anomalies and trends v3.0 product (2025), hereinafter XTRACK/ALES). The novel DSR is evaluated against six existing observation-selection algorithms applied to XTRACK and seven algorithms applied to XTRACK/ALES, and is validated across 272 TG stations globally for the period 2002–2020. Additionally, the capability of DSR to capture SLA signals is evaluated at various temporal scales – non-linear trend (interannual and trend), seasonal (annual), and residual at 264 stations for a longer study period 1994–2023. Finally, we investigate coastal sea level trends for the same period at 248 stations and analyse regional patterns.

https://doi.org/10.5194/egusphere-2026-4902
Preprint. Discussion started: 27 August 2026

2 Data and Methods

2.1 Data

2.1.1 Coastal altimetry products

Radar altimeter records the two–way travel time taken by radar pulses from satellite to sea surface and back, and is then converted to SSH using Eq. (1),

$$SSH = orbital\ altitude - (range + corrections)\ , \tag{1}$$

Here, $orbital\ altitude$ is the height at which the satellite flies with respect to the reference ellipsoid; $range$ is the distance calculated from the time of return of the echo; $corrections$ account for atmospheric effects on the propagation time.

Closer to the coast, the return signal contains signatures from land that enter the altimeter footprint, the quasi-specular reflections from calm water (like in the docks), steeper waves, and short-scale variability of sea surface characteristics (Vignudelli et al., 2011a). Yet, useful data can be retrieved by:

(1) Improving the range term by means of dedicated retracking algorithms for the coastal ocean during pre-processing (more effective for less than 10 km to the coast) (Vignudelli et al., 2011a).

(2) Improving the corrections term during post-processing (Vignudelli et al., 2011a).

The two main sources of altimeter data in this study are:

1. X-TRACK SLA L2P v2.2 (XTRACK): This product provides 1 Hz SLA for different altimeter missions such as TOPEX/Poseidon, Jason-1, Jason-2, Jason-3, SARAL/AltiKa, Envisat, ERS-1, ERS-2, Sentinel-3A, Geosat Follow-On (GFO), HaiYang-2A. In our study we chose TOPEX/Poseidon + Jason-1 + Jason-2 + Jason-3 + Sentinel-6A mission product which has the longest temporal availability of SLA time series (1993/02/28 to 2024/11/04). It has a temporal resolution of approximately 10 days, corresponding to the repeat cycle of the Jason series satellites and an along-track spatial resolution of 1 Hz (about 6-7 km between two consecutive along-track measurements). This product is AVISO L2P data (along-track sea level anomalies level-2+) post-processed using the X-TRACK program (described in Birol et al. (2017)). It employs an efficient editing strategy to minimize the loss of observations near the coast and refines the correction terms specifically for coastal areas. These corrections are statistically tested and recomputed using interpolation and extrapolation from datasets that provide local modelling of tides, atmospheric forcing, and wind stress.
2. Along-track sea level anomalies and trends v3.0 (2025) (XTRACK/ALES) (Cazenave et al., 2025): This product provides 20 Hz high-resolution monthly SLA dataset for Jason-1, Jason-2, and Jason-3 missions over the period January 2002 to June 2021, and the along-track spatial resolution is about 350 m. In this product, annual and semi-annual cycles of coastal SLA have been removed. The product is along-track altimetry observations pre-processed

https://doi.org/10.5194/egusphere-2026-4902
Preprint. Discussion started: 27 August 2026

using the ALES retracking strategy (Passaro et al., 2014) and post-processed using X-TRACK software (Birol et al., 2017). The ALES retracking improves the range term and thereby the SSH estimates. It does so by discarding the trailing edge of the signal waveform where most of the contamination happens, and fitting sub-waveforms based on the detected SWH. The sub-waveform width is adaptively adjusted to include the leading edge while minimizing contributions from the trailing edge, thereby enhancing the reliability of the range estimation. For more details on ALES strategy, see Passaro et al. (2014).

We retain all standard geophysical corrections already applied to the coastal altimetry products, including tidal correction and Dynamic Atmospheric Correction (DAC), for comparison.

TG data represents true monthly SLA mean values as it observes sea level at hourly intervals. In contrast, satellite altimetry missions such as SARAL/AltiKa (35-day repeat cycle), Sentinel-3A (27-day repeat cycle), and the TOPEX/Poseidon + Jason series (10-day repeat cycle) collect data less frequently. This difference in temporal sampling can impact the ability of altimeters to capture sea level variations accurately. Birol et al. (2021) highlighted that using only one observation per month can degrade the correlation between otherwise identical time-series, reducing it from 1 to 0.7 on average. For these reasons, we chose the TOPEX/Poseidon and Jason series satellites, not only for their frequent observations (3-4 observations per month) but also for the long time-series they provide, which is crucial for comparing sea level variations at different temporal scales with TG data.

2.1.2 Tide Gauge

The in-situ TG data is obtained from the Permanent Service for Mean Sea Level (PSMSL). The monthly Revised Local Reference (RLR) sea level data is used. In addition, ellipsoidal height links available for some stations from various GNSS solutions, also provided by PSMSL, are used.

2.1.3 DAC and VLM products

The Dynamic Atmospheric Correction (DAC) using ERA5 product is downloaded and is used to correct atmospheric perturbations on the TG sea level observations. DAC data is available as a gridded product having a spatial resolution of 0.125°×0.125° at hourly temporal resolution. Monthly means are calculated using simple arithmetic means from the hourly data at each grid point. For the DAC correction of TG sea level, we consider the nine closest grid points to the station and select the one that provides the highest variance reduction in the DAC corrected sea level (Dettmering et al., 2021).

Estimates of VLM corrections from GPS are also applied at each TG station. We flag stations where VLM estimate quality is poor. We do not include these stations for trend estimation. The VLM product used here is produced and distributed by the Nevada Geodetic Laboratory (NGL) (Blewitt et al., 2016; Hammond et al., 2016).

https://doi.org/10.5194/egusphere-2026-4902
Preprint. Discussion started: 27 August 2026

2.1.3 Bathymetry product

GEBCO_2025 is a gridded global bathymetry dataset with a 15 arc-second (15″) resolution and is used in this study to estimate the shelf-break along the global coastline. Preprocessing is carried out in QGIS, where the 200 m isobath is extracted using the "Contour" tool. Contours with an area smaller than 250 km² are filtered out and discarded. This is not applied to minor islands (table of minor islands is provided in Table S1 in Supplement). Further, contours with an area between 250 km^2 and 400,000 km^2 that appeared spurious are also discarded. This exercise is employed to remove artifacts in the GEBCO bathymetry grids.

2.2 Methods

2.2.1 Station Selection Criteria

The TG stations selected for the study must satisfy the following criteria.

The criteria for inter-algorithm comparison of XTRACK and XTRACK/ALES are,

1. TG observations available from 2002: Aligns with the start of XTRACK/ALES data availability, which begins in 2002 with the Jason-1 satellite mission.
2. Complete data coverage for 19 years (January 2002–December 2020): Fixes the study period to ensure consistency when comparing across different selection algorithms.
3. Data gap should not be more than 20% for the study period considered: Ensures continuity in the SLA time-series.
4. Only stations with satellite observations available within 100 km of the TG from both coastal altimetry products (XTRACK and XTRACK/ALES) are chosen: We select 100 km because XTRACK/ALES uses more stringent editing, resulting in the exclusion of several satellite observations, and we aim to include only those stations having observations within a 100 km radius.
5. Any station with a continuous data gap of 4 months or more in the time-series should be excluded: Prevents long gaps in the time-series.

After applying these criteria, 272 TG stations remained for comparison with in-situ TG measurements. We apply seven different selection algorithms separately to XTRACK/ALES and XTRACK to compute coastal SLA, with the novel DSR among those applied to XTRACK. The compared signal is the detrended deseasonalized SLA, in accordance with the TG validation methodology followed by Cazenave et al. (2022).

To evaluate the performance of DSR-applied XTRACK in capturing sea level variability at various temporal scales and in estimating coastal sea level trends, we use a longer time-series from 1994 to 2023. We use the same criteria as before, with the following modifications: TG observations must be available from 1994, with complete data coverage for 30 years, and stations with satellite observations within 300 km from the TG. The data gap criteria (no more than 20% missing data, and no continuous gap exceeding 4 months) remains unchanged. After applying these criteria, a total of 264 TG stations remain.

https://doi.org/10.5194/egusphere-2026-4902
Preprint. Discussion started: 27 August 2026

2.2.2 Intercomparison algorithms

Table 1 Altimetry selection algorithms from literature and their adapted variants to compare against the novel DSR.

Coastal altimetry product	Algorithm	Description	Label
XTRACK	Fixed Search Radius	The mean of all altimetry observations inside an SR of 150 km centered on TG.	X_150
		The mean of all altimetry observations inside an SR of 200 km centered on TG.	X_200
		The mean of all altimetry observations inside an SR of 250 km centered on TG.	X_250
		The mean of all altimetry observations inside an SR of 300 km centered on TG.	X_300
	Nearest Pass 250 km	The mean of all altimetry observations from the nearest pass and within 250 km from the TG.	X_np250
	Nearest Point	The nearest altimetry observation having 80% completeness in its time series is chosen.	X_npoint
XTRACK/ALES	Fixed Search Radius	The mean of all altimetry observations inside an SR of 200 km centered on TG.	ales_200
	Nearest Pass	The mean of all altimetry observations from the nearest pass to the station.	ales_npass
	Nearest Two Passes	The mean of all altimetry observations from the nearest two passes to the station.	ales_2npass

https://doi.org/10.5194/egusphere-2026-4902
Preprint. Discussion started: 27 August 2026

	Nearest Site inside 300 km Search Radius	A 300 km SR may pick observations from a different coast. Thus, for each pass (pass-number), we retain only the nearest site (station-number) and compute the mean across all passes.	ales_300
	Nearest 10 observations mean	The mean of 10 nearest observations from the station.	ales_n10pt
	Nearest 10 observations mean filtered	The filtered mean of 10 nearest observations from the station.	ales_filt_np
	Nearest Point	The nearest altimetry observation having 80% completeness in its time-series is chosen.	ales_np

2.2.3 Time Series Decomposition, Trend Estimation and Statistical Metrics

We perform outlier removal for TG measurements using the median absolute deviation method (Hampel, 1974), however, XTRACK and XTRACK/ALES require no additional preprocessing as outliers are already removed during their processing. For all comparisons, we require at least 80% completeness in the time-series, and comparisons are made only when this condition is met (Birol et al., 2021; Mohamed et al., 2019; Prandi et al., 2009).

The XTRACK/ALES product is delivered with annual and semi-annual signals already removed using a least-squares fit to a sinusoidal function during its processing. Hence, for inter-algorithm comparison, we apply the same method to TG and XTRACK SLA time series, ensuring all three datasets are deseasonalized consistently. The trend is then computed using ordinary least squares (OLS) simple regression fit and removed. We use statistical metrics such as Pearson correlation coefficient (r), and Normalized Root Mean Square Error (NRMSE) for the comparison of detrended deseasonalized SLA. We normalize Root Mean Square Error (RMSE) using the standard deviation of TG SLA. The value of the NRMSE represents the ratio between the variation not explained by the altimetry SLA and the overall variation in TG SLA. If the altimetry SLA time-series explains a fraction of the variation but leaves out some part, which is at a similar scale to the overall variation, the ratio will be around 1. If NRMSE is greater than 1, this indicates greater variation or noise in the altimetry SLA.

https://doi.org/10.5194/egusphere-2026-4902
Preprint. Discussion started: 27 August 2026

For evaluating DSR algorithm performance at multiple temporal scales, we perform the Seasonal and Trend decomposition using LOESS (STL) on time-series and analyse non-linear trend (NLT), residual, and annual signals. STL is chosen because it is resilient to transient outliers and allows annual amplitudes and trends to vary over time (Cleveland et al., 1990). NLT includes low-frequency signals such as interannual variability and linear trend, the residual signal captures monthly to interannual signals, and the annual signal represents the seasonal variability in the sea level anomalies. We validate against TG by measuring r, and RMSE at each of these temporal scales.

After removing stations that are not corrected for VLM, the linear coastal sea level trends for the period of 1994 to 2023 (30 years) are estimated using OLS linear regression at 248 stations along the global coastline. The uncertainty of the trends is given at the 95% confidence interval, and only trends with a p-value < 0.05 are considered significant and reported. A paired t-test is also performed to determine whether the mean difference between the two sets of observations is zero.

2.2.4 Ellipsoidal Correction

We analyse the performance of DSR with TG linked to the ellipsoid. Sea level measured by the TG is with respect to a local datum, whereas altimetry measures SSH above the reference ellipsoid, WGS84. Since we use Revised Local Reference (RLR) data from PSMSL, the stability of the local datum is ensured by fixing its height to a tide gauge benchmark (TGBM), which is assumed to be on stable ground. In our analysis, we correct for VLM using GPS data and then remove the long-term mean from sea level to obtain the SLA, which is then compared with altimetry-derived SLA. As we are comparing the SLA time-series, any effect due to the different reference levels is assumed to be negligible. However, for further analysis, we select stations with information on ellipsoidal links from PSMSL (Stations with Ellipsoidal Links, 2026). Ellipsoidal links are estimated using continuous GNSS measurements from different GPS solutions such as ULR7a, JPL14, NGL14, and GT3. All these solutions use GRS80 as the reference ellipsoid. We acquire 49 stations referred to the ellipsoid for comparison with altimetry across different temporal scales. We apply ellipsoid correction as,

$$SSH_{elip} = SSH_{RLR} + H_{RLR} , \tag{2}$$

Here, SSH_{elip} is the SSH above the ellipsoid, SSH_{RLR} is the SSH referred to the RLR TG datum, and H_{RLR} is the height of the RLR datum above the ellipsoid. Additionally, this SSH is corrected for VLM using GPS solutions. This correction is necessary because, in Eq. (2), the RLR datum is assumed to be stable, which may not be true due to VLM. Further, we estimate bias between SLA from TG referenced to the ellipsoid and altimetry using Student's *t*-test.

https://doi.org/10.5194/egusphere-2026-4902
Preprint. Discussion started: 27 August 2026

3 The Dynamic Search Radius algorithm

3.1 Algorithm Formulation

The shelf-width and its gradient play a dominant role in coastal sea level dynamics, thus including this information appears to be vital in the selection of altimetry observations that would best capture the coastal sea level changes, but is not considered in the existing algorithms. Hence, a new selection algorithm is proposed that considers altimetry observations falling inside the shelf-break. Shelf-break is defined as the location where the continental shelf meets the continental slope. Although found to exhibit a wide variability, it is commonly defined at the 200 m isobath (Akpinar et al., 2022; Negroni et al., 2025) or at the 34.5 isohaline (Hirzel et al., 2023; Linder and Gawarkiewicz, 1998).

Several studies over various disciplines and across different coasts approximate the shelf-break at 200 m isobath (Allen, 2004; J. N. Druon et al., 2001; Franco et al., 2022, 2017; Fratantoni and Pickart, 2003; Gawarkiewicz et al., 2012; Graham et al., 2018; Johnson et al., 2023a; Siedlecki et al., 2011; Skov and Durinck, 1998; Todd et al., 2013; Zhang et al., 2017; Zhao and Guo, 2011a). For example, Graham et al. (2018) assessed the strength of downwelling circulation around the European northwest shelf across the shelf-break defined at 200 m isobath, while Franco et al. (2017) showed long-term trends of sea surface temperature, chlorophyll-a, and absolute dynamic topography in the Patagonian shelf-break front, also along the 200 m isobath from GEBCO.

Additional studies over various fields, including temporal stability of the concentration of seabirds at the North Sea shelf-break fronts in Skagerrak (Skov and Durinck, 1998), relation between southwest and northeast winds at the southeast coast of Aotearoa (Johnson et al., 2023b), effect of upwelling on the production of phytoplankton at the shelf-break fronts along the Mid-Atlantic Bight (Negroni et al., 2025), temporal evolution of cross-shelf exchanges and importance of eddy induced component of cross-shelf transport in Black Sea (Akpinar et al., 2022), examination of supply of oceanic nutrients to the East China Sea shelf-break (Zhao and Guo, 2011b), investigation of weak flow across shelf-break due to deep cross-shelf flow at the west coast of Vancouver Island (Allen, 2004), quantification of the influence of vertical mixing enhanced by the internal waves in the shelf-break region of Brittany in the Bay of Biscay (Druon et al., 2001a), all defines shelf-break at 200 m isobath. Accordingly, this study defines the shelf break at the 200 m isobath, which is therefore suitable for global analysis.

In the first step of the algorithm, points along the coastline are selected, extending 15 km (parameter #1, called as coastline extent) on either direction from the TG location. Next, the maximum width of the shelf-break within the coastline extent is calculated and designated as the first Search Radius (SR1) for that TG. The mean of altimetry observations inside this SR1 represents the coastal SLA. While aggregating, altimetry points with less than 80% completeness in their time-series are excluded (Birol et al., 2021; Mohamed et al., 2019; Prandi et al., 2009). Further, we set a lower limit of 15 altimetry points to be present within SR1; defined as the threshold (parameter #2). If this condition is not satisfied, the SR is updated to 250 km, defined as SR2 (parameter #3), and altimetry points only inside the shelf-width (maximum shelf-width (value of SR1)) are selected. Then the mean SLA from the selected observations is calculated. This ensures the collection of observations from

https://doi.org/10.5194/egusphere-2026-4902
Preprint. Discussion started: 27 August 2026

different passes and thus better temporal sampling. For instance, the altimetry SLA for the station Brest is produced using data from four satellite passes (see Fig. 1). If the threshold is still not satisfied, we believe that not many observations are available to find altimetry SLA, and we discard that station from further analysis. Since the width and depth of shelf is found to be dramatically varying along the coastline (Paris et al., 2016), we use the largest width of the shelf-break inside the coastline extent (extending 15 km on each side of the TG (since parameter #1 =15 km)), which allows us to capture most of the observations along the coast but within the shelf over that region. The values of the three parameters are shown to be robust and meaningful through a sensitivity analysis (SA) spanning 396 parameter combinations across 318 TG stations (see Section 3.2., Figs. B1–B3 in Appendix B). Since the SR is dynamic and is decided for each TG based on the nearby shelf-break, it is called the Dynamic Search Radius algorithm. An illustrative explanation of the algorithm is shown in Fig. 1. The flowchart in Fig. 2 depicts the overall workflow used to prepare the altimetry (using DSR) and TG datasets for comparison.

This algorithm is not applied on TG installed on minor islands as they are primarily surrounded by open ocean (depths > 200 m) and the coastal shelf is very narrow. However, to include minor islands in the global assessment of coastal altimetry, a fixed SR of 200 km is chosen, to calculate the mean of all the altimetry observations for that island station.

https://doi.org/10.5194/egusphere-2026-4902
Preprint. Discussion started: 27 August 2026

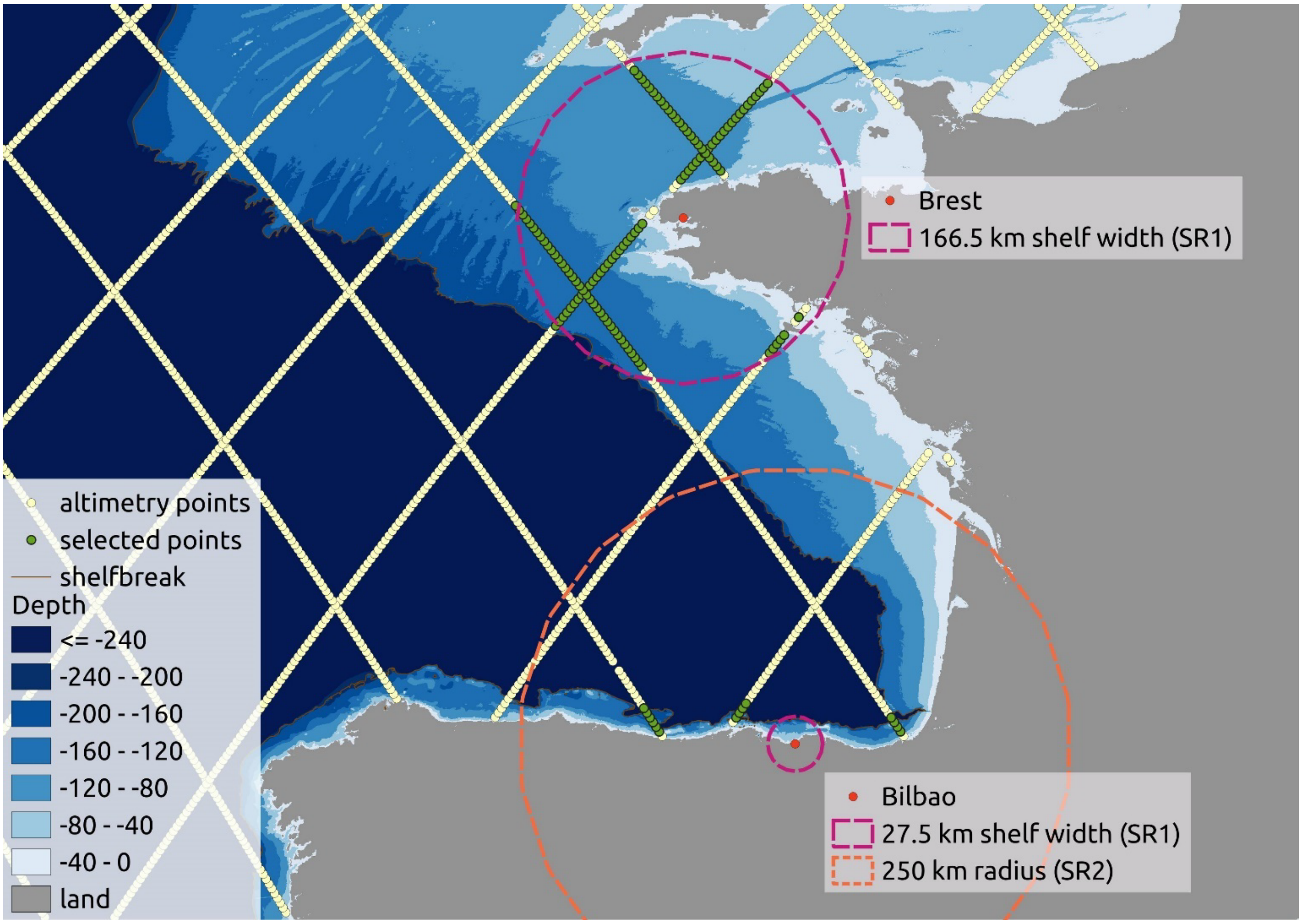

Figure 1 Illustrative example of DSR. At station Brest (station ID-1), SR1 is 166.5 km which is the maximum shelf-width along the coastline extent of 15 km from the station. Here, upon satisfying the criteria of threshold (15 observations), all observations inside SR1 are selected (green circles). At station Bilbao (station ID-1806), due to insufficient observations (less than threshold) with SR1 (27.5 km), SR2 of 250 km is used and satellite observations only within the coastal shelf is selected (green circles). Red circles represent the tide gauge stations and light-yellow circles are altimetry observations. Note that some altimetry points although within the shelf are not selected, since they do not meet the 80% completeness criterion in its time series.

https://doi.org/10.5194/egusphere-2026-4902
Preprint. Discussion started: 27 August 2026

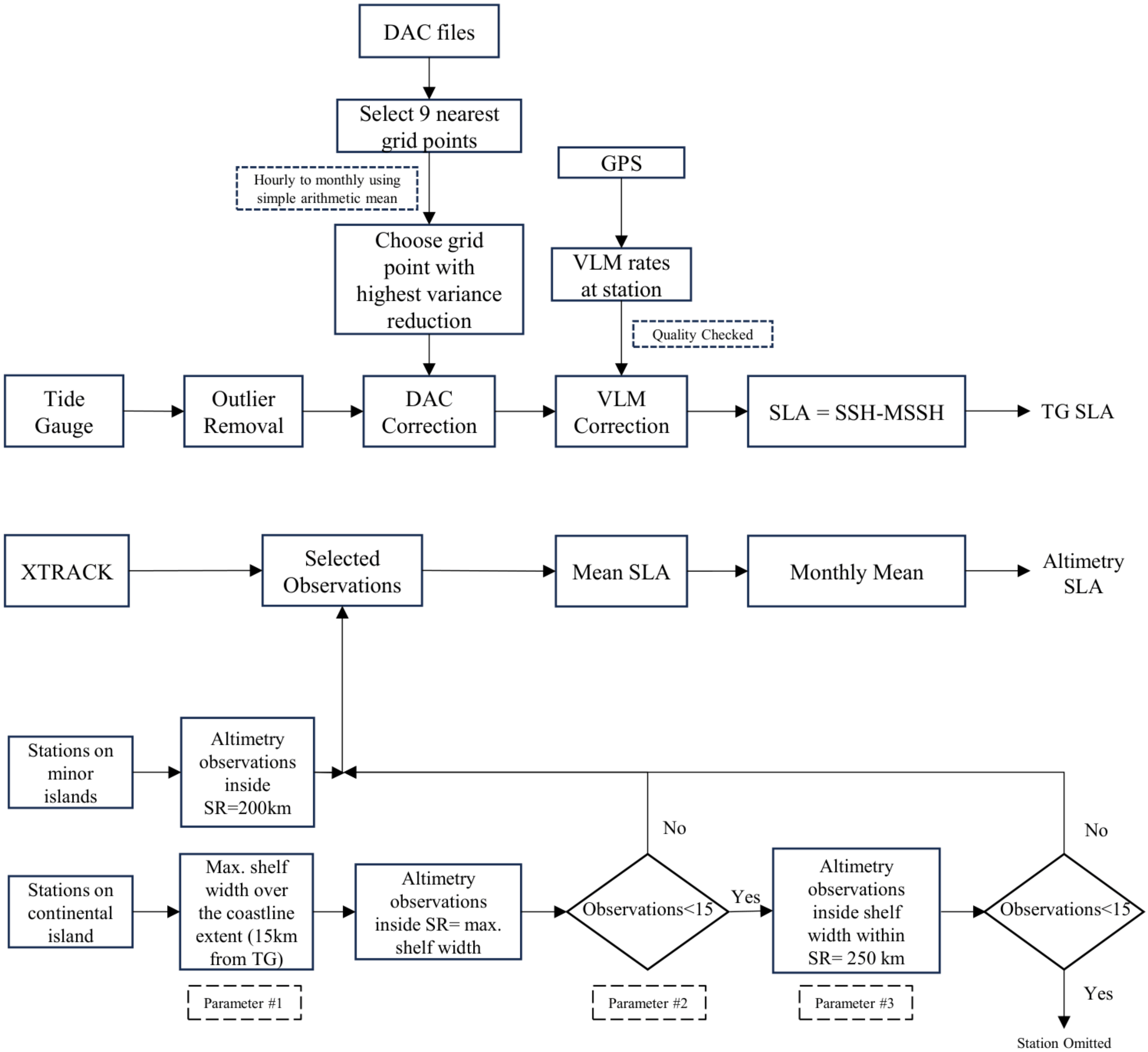

Figure 2 Schematic overview of the DSR algorithm, including TG data preprocessing, outlining the workflow used to prepare altimetry and TG datasets for comparison.

3.2 Sensitivity to parameter choice and uncertainty estimation

DSR's performance is sensitive to the parameters chosen – (1) coastline extent, (2) threshold, and (3) SR2 – that determine which altimetry observations are chosen. The suggested values for these parameters are varied to find their impact on overall

https://doi.org/10.5194/egusphere-2026-4902
Preprint. Discussion started: 27 August 2026

performance. The coastline extent is allowed to vary from 1 km, then 5 to 50 km in 5 km increments, threshold from 1, then 5 to 25 in steps of 5, and SR2 from 100 to 350 km in 50 km increments. Hence, we test 396 parameter combinations across 312 TG stations for the period 1994 – 2023 (see Fig. B1-B3, in Appendix B). After applying the DSR algorithm using each of the 396 parameter combinations, we perform time series decomposition using STL Loess and compute r and RMSE between altimetry and TG for NLT, seasonal, and residual signals. The first filtering step removes parameter combinations that discarded more than 15% of total stations, reducing the set from 396 to 242 combinations. For each remaining combination, we calculate the percentage of stations with $r^2 \geq 0.64$ (explaining at least 64% of variance), and the percentage of stations with RMSE ≤ 20 mm for NLT, residual, and annual signals. Based on the r^2 of NLT signal (Fig. B1(a)), coastline extent of 1 km is removed. Based on the RMSE of NLT signal (Fig. B1(b)), coastline extent of 35 km is removed. Based on the r^2 of residual signal (Fig. B2(a)), SR2 values of 100 km and 150 km are removed, threshold of 1 is removed and coastline extents of 30 km, 40 km, 45 km are removed. Based on the RMSE of the residual signal (Fig. B2(b)), SR2 value of 300 km is removed and coastline extent of 25 km is removed. Based on the r^2 of the annual signal (Fig. B3(a)), the thresholds of 5 and 10 are removed. Based on the RMSE of the annual signal (Fig. B3(b)), threshold of 25 is removed and coastline extents of 5 km and 50 km are removed.

After these filtering steps, six parameter combinations remained. Our chosen parameter combination – a threshold of 15, coastline extent of 15 km, and SR2 of 250 km – is among them (highlighted with a red circle in Fig. B1–B3). Please note that the performance does not vary significantly across the six combinations. Table B1 in Appendix B shows the six parameter combinations remaining after filtering the 396 combinations.

Additionally, to test the robustness of the algorithm, uncertainty in r at each station is estimated using the Fisher Z-transformation (Bhowmik and Sankarasubramanian, 2019). We can conclude that the suggested parameters offer the best performance for implementing the DSR algorithm.

4. Results and Discussions

4.1 A comprehensive validation and assessment of DSR

The novel DSR, along with other popular approaches, such as fixed SR, nearest pass, and nearest observation, is compared against TG observations at 272 stations for 2002-2020. The performance of altimetry against TG is assessed using r and NRMSE. An altimetry observation is considered to exhibit good agreement with TG data if the r exceeds 0.7, or the NRMSE is below 1. The XTRACK/ALES product provides deseasonalized SLA. Hence, to facilitate the intercomparison of XTRACK with TG and XTRACK/ALES, annual and semi-annual signals are removed from TG and XTRACK. The detrended deseasonalized (DeST) SLA are then compared, with the linear trend being removed using least-squares regression.

https://doi.org/10.5194/egusphere-2026-4902
Preprint. Discussion started: 27 August 2026

The stations are grouped based on their coastal region: Indian Ocean–South China Sea (IO-SCS), Gulf of Mexico (GoM), eastern Australia (EAus), western Australia (WAus), South America (SA), Pacific Islands (PI), northwest America (NWA), North Sea (NSea), north Pacific Ocean (NPO), New Zealand (NZ), northeast Atlantic Ocean (NEAt), Mediterranean Sea (MedSea), Baltic Sea (Baltic) as shown in Fig. 3(c). Box plots of r and NRMSE are shown in Fig. 3(a, b) and Fig. 4(a, b), respectively.

DSR consistently outperforms other algorithms across most regions, with median r value of 0.97 (Baltic), 0.75 (Eaus), 0.79 (GoM), 0.72 (IO_SCS), 0.71 (NEAt), 0.84 (NSea), 0.71 (NZ), 0.51 (SA), 0.92 (WAus) (Fig. 3). It performs comparably with XTRACK/ALES algorithms in several regions: MedSea (0.77 for DSR, compared to 0.79 and 0.78 for ales_300 and ales_200), NEA (0.75 for DSR and 0.76 for ales_300), NPO (0.74 for DSR and 0.76 for ales_300), NWA (0.84 for DSR and 0.85 for ales_300) and PI (0.86 for DSR and 0.89 for ales_300 and ales_200) (Fig. 3(a)).

All XTRACK/ALES algorithms show poor performance in IO-SCS region. Among the XTRACK/ALES and XTRACK algorithms, the nearest point method (ales_np and X_npoint) consistently gives poor performance across all coastal regions (Fig. 3(a, b)). It is worth noting that for coastal regions such as EAus, NPO, IO-SCS, and NZ, the DSR algorithm performs notably better than any algorithm applied to the high-resolution product (Fig. 3(b)). In fact, with the exception of NSea, DSR is the only algorithm achieving a median $r \geq 0.7$ in these regions. Among all the XTRACK/ALES algorithms, ales_300 performs the best. The nearest virtual station from XTRACK/ALES (ales_np) falls behind X_DSR in most regions, showing a median r of 0.85 (0.97 for X_DSR) in Baltic, 0.56 (0.75) in EAus, 0.66 (0.79) in GoM, 0.46 (0.72) in IO-SCS, 0.67 (0.77) in MedSea, 0.62 (0.75) in NEA, 0.54 (0.71) in NEAt, 0.65 (0.74) in NPO, 0.62 (0.84) in NSea, 0.8 (0.84) in NWA, 0.3 (0.71) in NZ, 0.44 (0.51) in SA, and 0.84 (0.92) in WAus. However, in PI, ales_np performs slightly better than X_DSR, with median r values of 0.87 (0.86).

When comparing all XTRACK algorithms, DSR performs notably better than any other in coastal regions such as NEAt, NPO, NWA, NZ, and WAus – particularly in NEAt, NPO, and NZ, where DSR is the only XTRACK algorithm with a median $r \geq 0.7$. Closer examination reveals that stations located along narrow shelves in these three regions show improved performance with DSR, suggesting that retrieving observations along the coast but inside the shelf-break improves performance. For example, compared with X_200, DSR shows improved performance ($r \geq 0.7$) at 69 stations, most of which are located along narrow shelves.

https://doi.org/10.5194/egusphere-2026-4902
Preprint. Discussion started: 27 August 2026

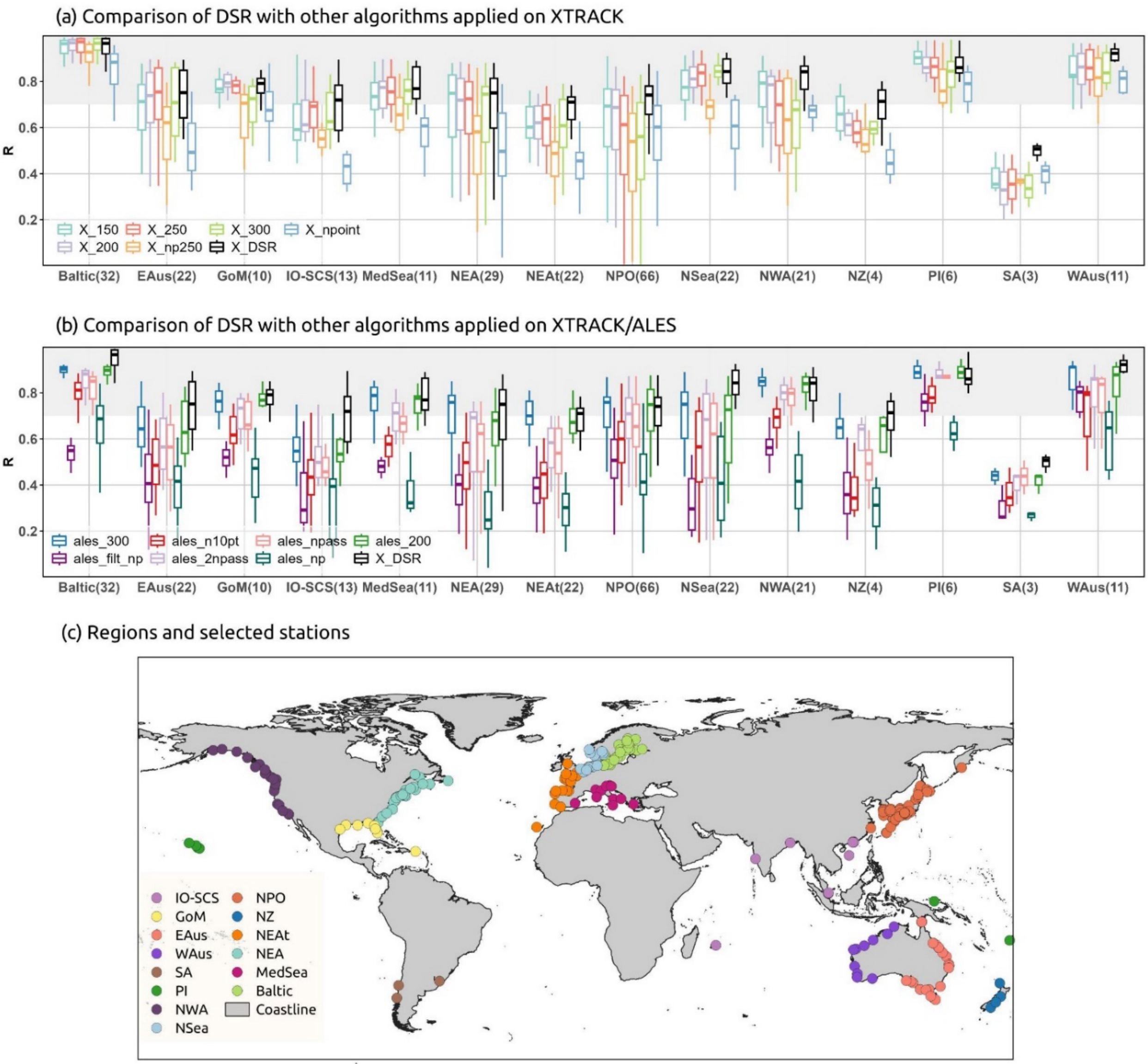

Figure 3 Evaluation of different algorithms for representing coastal sea level variability. (a) shows DSR (X_DSR) for XTRACK product compared with six alternate algorithms applied on XTRACK: X_150, X_200, X_250, X_np250, X_300, and X_npoint. (b) shows DSR (X_DSR) compared with seven alternate algorithms applied on XTRACK/ALES: ales_300, ales_filt_np, ales_n10pt, ales_2npass, ales_npass, ales_np, and ales_200. The comparison is based on correlation coefficient (r) and is conducted at 272 TG stations. Box plots of region-wise r is shown, with r ≥ 0.7 considered as good agreement, shaded in grey. Regions are shown on the y-axis, with the number of stations in each region indicated in parentheses next to the region name. (c) shows stations from different regions as colored circles, with each color representing a specific region. Region abbreviations: EAus- eastern Australia, GoM- Gulf of Mexico, IO-SCS- Indian Ocean-South China Sea, MedSea-

https://doi.org/10.5194/egusphere-2026-4902
Preprint. Discussion started: 27 August 2026

Mediterranean Sea, NEA- northeast America, NEAt- northeast Atlantic Ocean, NPO- north Pacific Ocean, NSea- North Sea, NWA- northwest America, NZ- New Zealand, PI- Pacific Islands, SA- South America, WAus- western Australia.

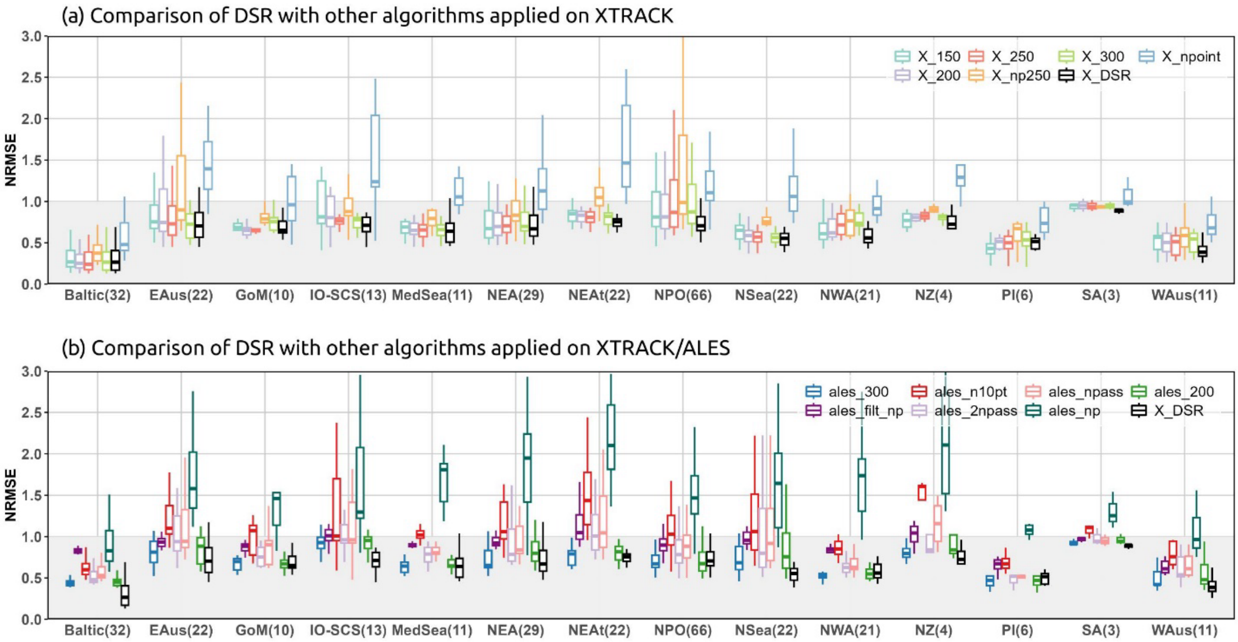

Figure 4 Evaluation of different algorithms for representing coastal sea level variability. (a) shows DSR (X_DSR) for XTRACK product compared with six alternate algorithms applied on XTRACK: X_150, X_200, X_250, X_np250, X_300, and X_npoint. (b) shows DSR (X_DSR) compared with seven alternate algorithms applied on XTRACK/ALES: ales_300, ales_filt_np, ales_n10pt, ales_2npass, ales_npass, ales_np, and ales_200. The comparison is based on NRMSE and is conducted at 272 TG stations. Box plots of region-wise NRMSE is shown, with NRMSE<1considered as good agreement, shaded in grey. Regions are shown on the y-axis, with the number of stations in each region indicated in parentheses next to the region name. Region abbreviations: EAus- eastern Australia, GoM- Gulf of Mexico, IO-SCS- Indian Ocean-South China Sea, MedSea- Mediterranean Sea, NEA- northeast America, NEAt- northeast Atlantic Ocean, NPO- north Pacific Ocean, NSea- North Sea, NWA- northwest America, NZ- New Zealand, PI- Pacific Islands, SA- South America, WAus- western Australia.

4.2 Comparing XTRACK/ALES and XTRACK with TG data

We analysed DeST signal of coastal SLA at 373 stations for the time period 2002-2020 using DSR-applied XTRACK and ales_300 algorithm-applied XTRACK/ALES. We found 272 stations (~70%) show good correlation with XTRACK (X_DSR) (Fig. 5(a)), compared to 231 (~62%) with XTRACK/ALES (ales_300) (Fig. 5(b)) in capturing DeST SLA. The DeST signal represents the residual, which includes low-frequency signals such as interannual and various monthly to interannual signals.

https://doi.org/10.5194/egusphere-2026-4902
Preprint. Discussion started: 27 August 2026

While DeST may still retain signatures of storm surges, these are likely to be significantly damped at monthly scales. Instead, the remaining variability (excluding the influence of atmospheric pressure) probably reflects processes such as SLA driven by local-wind forcing, remote forcing that induces mass fluxes, and sea level variability due to coastal trapped waves (Wise et al., 2024). We find good agreement with TG from X_DSR at Long Island Sound situated between Chesapeake Bay and Bay of Fundy, western and southern Australia, Norwegian coast, Baltic Sea, Queen Charlotte Sound, Gulf of Mexico, northwest America, and North Sea beyond the Strait of Dover.

Observations at stations on the western coast of Australia demonstrate stronger correlation and lower RMSE, however, along the eastern coast, we find lower correlation and higher RMSE. Notably, altimetry fails to capture the DeST signal, even for observations taken within the shelf-break and as close as 10 km from the TG. Similar findings are reported in a recent study by Benveniste et al. (2020). This discrepancy can be attributed to the Eastern Australian Current (EAC), which flows near the coast and is associated with highly variable mesoscale EAC eddies (Benveniste et al., 2020). Station Eden is located in the Twofold Bay, lying at the confluence of two oceanic boundaries – the near end of EAC and the Southern Ocean. We find observations selected along the southern Australian coast, 200 km away, capture the sea level variability better than observations in the eastern coast (Fig. 6).

Stations located in the Gulf of St. Lawrence generally exhibit poor correlation. We also observe poor correlation at stations located in tidally dominated estuaries, such as Kanmen (in the Oujiang Estuary), and Mar del Plata and Montevideo (both in the Rio de la Plata Estuary). However, this is not always the case. Prince William Sound, one of the largest estuaries in North America, is supplied by rivers and numerous tide-water glaciers, with circulation thought to be primarily tidally driven. For the two stations in this sound — Cordova (east side) and Valdez (near the head of a deep fjord) — no observations were available within the sound itself. DSR instead selects observations up to 100 km away, outside the sound but within the shelf, yielding good agreement at both stations (Cordova: $r = 0.91$, RMSE = 20.8 mm; Valdez: $r = 0.88$, RMSE = 25.3 mm). Stations Skagway (Lynn Canal) and Juneau (Gastineau Channel) are located in the narrow channels of the Inside Passage, in the northwest Pacific, where altimetry observations are not available. The nearest observations lie outside the passage, inside the shelf-width. Station Sitka, located on the shelf around 150 km from Juneau, outside the Inside Passage, obtains good correlation ($r = 0.8$) and low RMSE (27.9 mm). For Skagway and Juneau, the difference between altimetry and TG SLA is largest in October — which also corresponds to the month of maximum precipitation and, thus, maximum freshwater runoff — and smallest during April–May. Due to high precipitation and runoff, October is associated with high heat content and low salinity, whereas April–May is associated with low heat content and high salinity in Lynn Canal (McLain, 1969). This might be the reason for the discrepancy observed at these stations when offshore (inside the shelf-width) observations are selected.

https://doi.org/10.5194/egusphere-2026-4902
Preprint. Discussion started: 27 August 2026

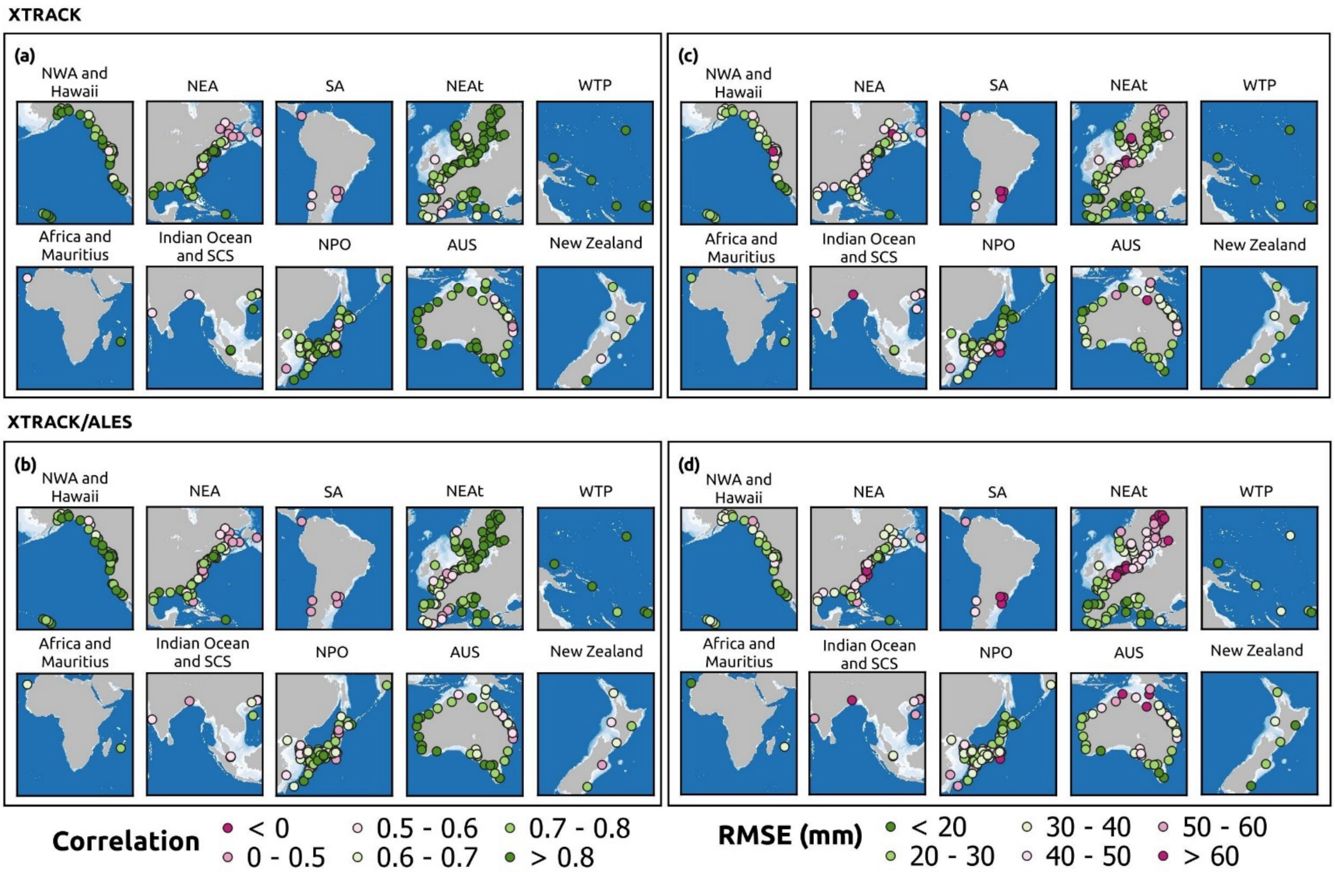

Figure 5 Validation of XTRACK (X_DSR) with XTRACK/ALES (ales_300): Correlation and RMSE with TG. Circles represent TG stations, with circle color indicating the correlation and RMSE. Shades of pink indicate poor correlation and large RMSE, while shades of green represent good correlation and low RMSE. (a) and (c) show correlation and RMSE of XTRACK with TG, while (b) and (d) show correlation and RMSE of XTRACK/ALES with TG. Regional abbreviations: NWA and Hawaii- northwest America and Hawaii, NEA- northeast America SA- South America, NEAt- northeast Atlantic Ocean, WTP- west tropical Pacific Ocean, Indian Ocean and SCS- Indian Ocean and South China Sea, NPO- north Pacific Ocean, AUS- Australia.

https://doi.org/10.5194/egusphere-2026-4902
Preprint. Discussion started: 27 August 2026

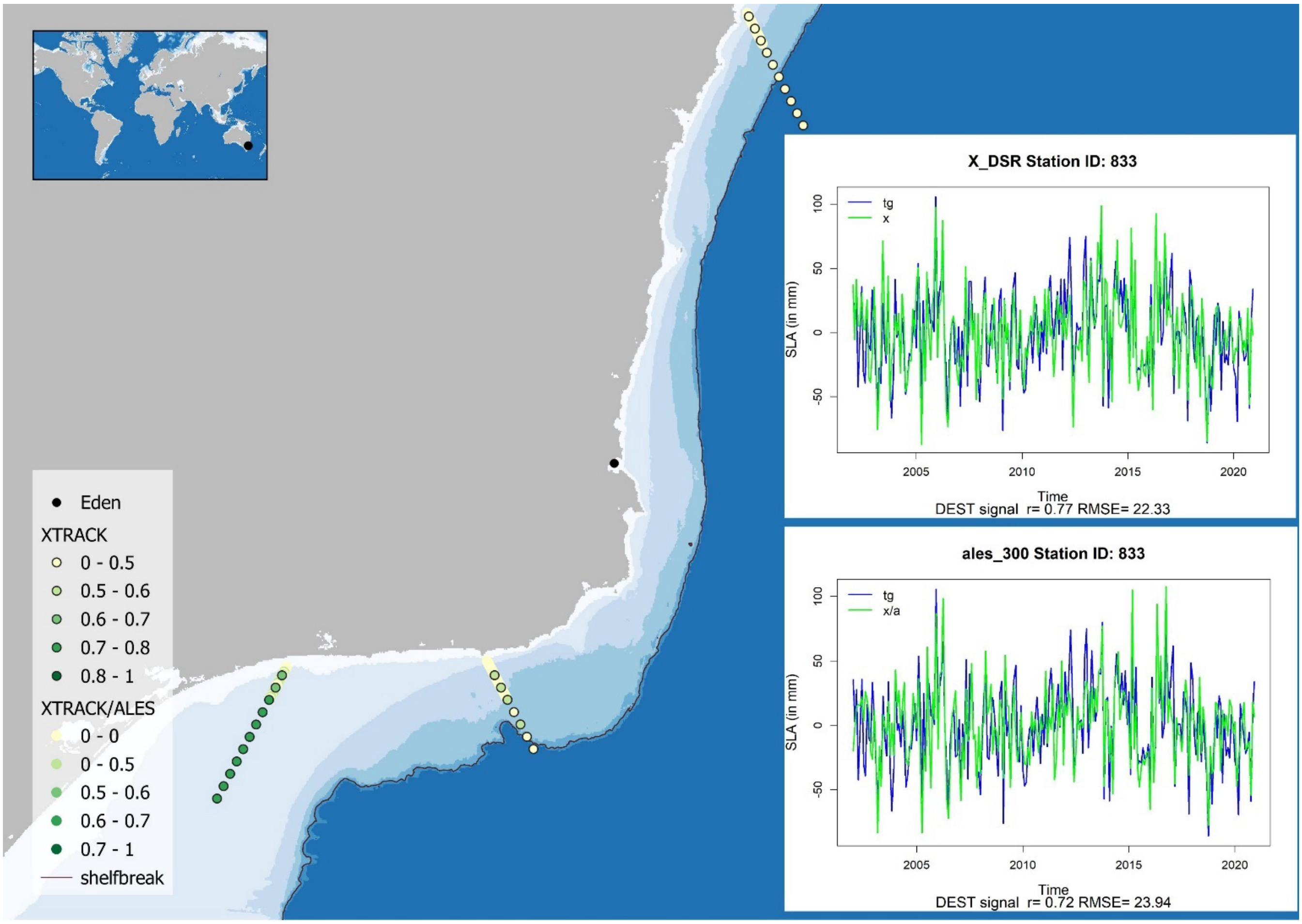

Figure 6 A deep dive into the capturing of sea level variability at station Eden. The figure illustrates altimetry observations from XTRACK/ALES 20 Hz (circles without solid outlines) and XTRACK 1 Hz (circles with solid outlines). The observations shown here are those selected using X_DSR algorithm and ales_300 algorithm. Colours represent correlation values between altimetry and tide gauge data, ranging from light yellow (low, 0) to dark green (high, 1). The accompanying time series shows coastal SLA from X_DSR, ales_300, and TG, with TG SLA shown in blue and altimetry SLA shown in green. The TG station Eden is represented by black circle. An inset map is included to show the geographic location of the station.

The high-resolution XTRACK/ALES (20 Hz) product performs better at narrow coasts due to its ability to retrieve observations closer to shore. However, the DSR algorithm now enables even the low-resolution (1Hz) XTRACK product to perform at par in these regions by taking observations along the coast rather than across the coast. For example, the Charleston II station located in the NWA, has a shelf-break distance of 37 km. Since the DSR algorithm takes observations along the coast and within the shelf-break, observations as far as 200 km are selected, resulting in r = 0.88 and RMSE =25.6 mm (Fig. 7).

https://doi.org/10.5194/egusphere-2026-4902
Preprint. Discussion started: 27 August 2026

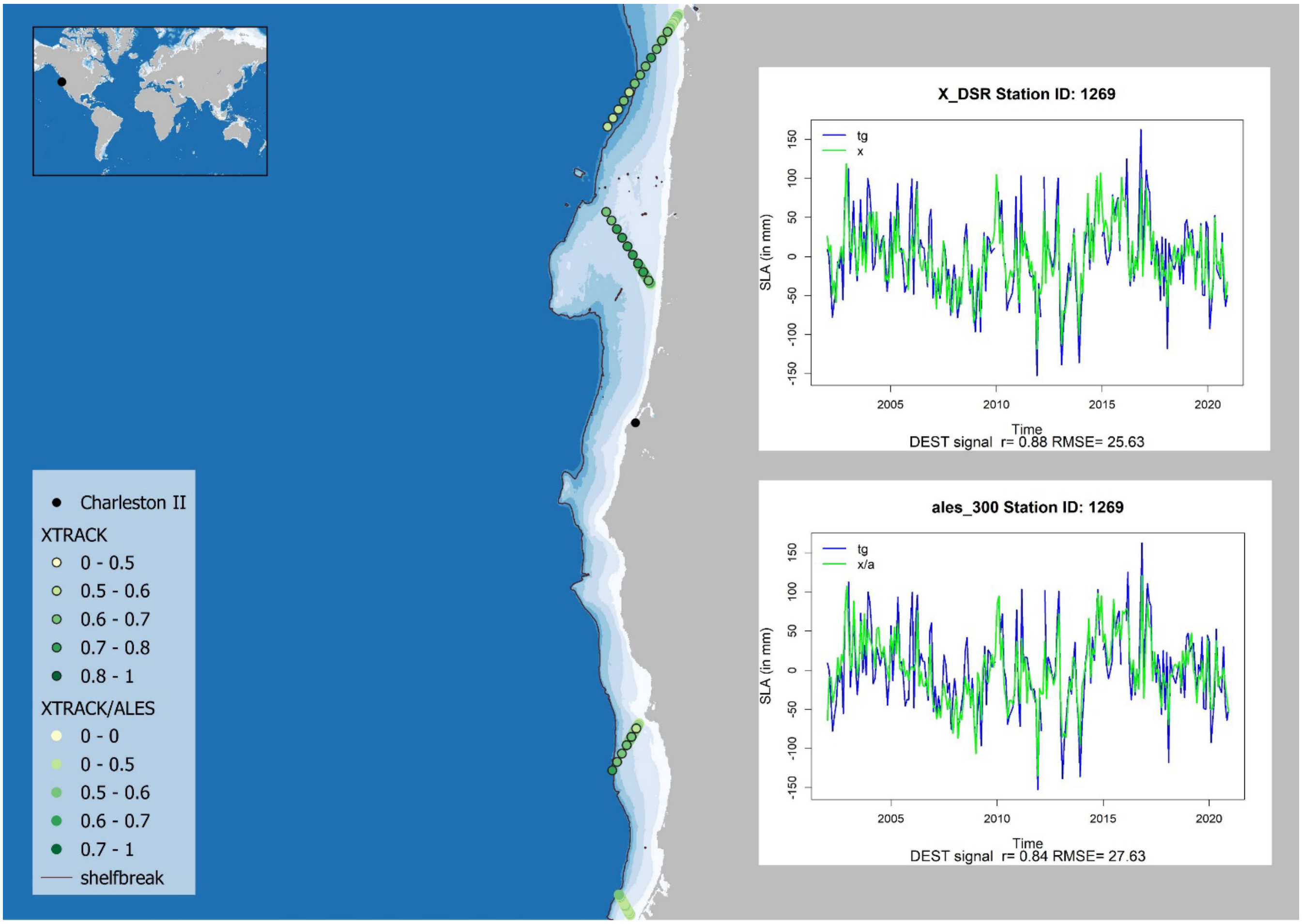

Figure 7 A deep dive into the capturing of sea level variability at station Charleston II. The figure illustrates altimetry observations from XTRACK/ALES 20 Hz (circles without solid outlines) and XTRACK 1 Hz (circles with solid outlines). The observations shown here are those selected using X_DSR algorithm and ales_300 algorithm. Colours represent correlation values between altimetry and tide gauge data, ranging from light yellow (low, 0) to dark green (high, 1). The accompanying time series shows coastal SLA from X_DSR, ales_300, and TG, with TG SLA shown in blue and altimetry SLA shown in green. The TG station Charleston II is represented by black circle. An inset map is included to show the geographic location of the station.

Station Trieste is located in the Gulf of Trieste, an area characterized by shallow shelf. There are no altimetry observations from the XTRACK product inside the Gulf. However, the DSR algorithm selects observations outside the Gulf of Trieste and captures the signal observed at the station, as shown in Fig. 8, with r = 0.89 and RMSE = 20 mm.

https://doi.org/10.5194/egusphere-2026-4902
Preprint. Discussion started: 27 August 2026

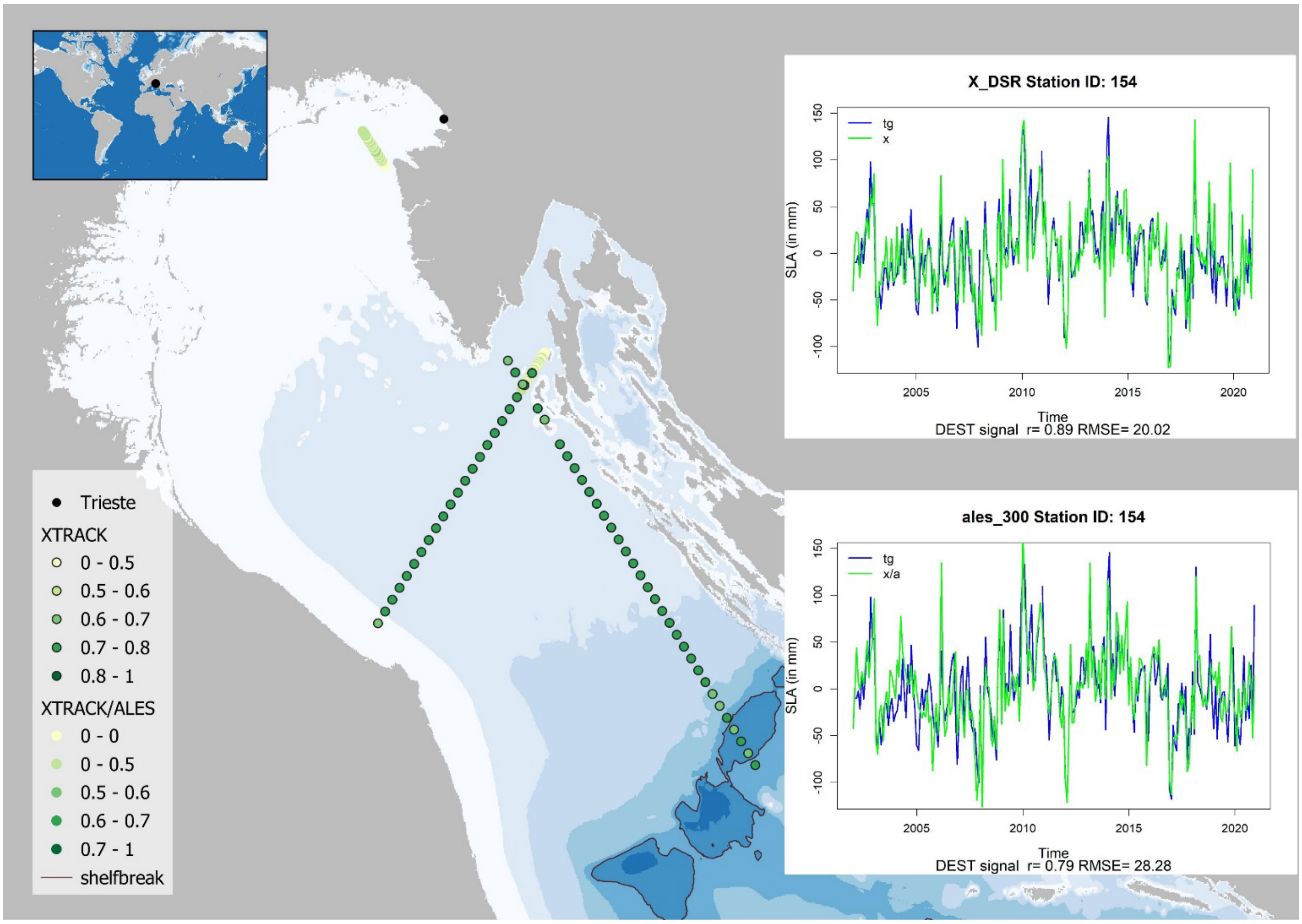

Figure 8 A deep dive into the capturing of sea level variability at station Trieste. The figure illustrates altimetry observations from XTRACK/ALES 20 Hz (circles without solid outlines) and XTRACK 1 Hz (circles with solid outlines). The observations shown here are those selected using X_DSR algorithm and ales_300 algorithm. Colours represent correlation values between altimetry and tide gauge data, ranging from light yellow (low, 0) to dark green (high, 1). The accompanying time series shows coastal SLA from X_DSR, ales_300, and TG, with TG SLA shown in blue and altimetry SLA shown in green. The TG station Trieste is represented by black circle. An inset map is included to show the geographic location of the station.

4.3 DSR-applied XTRACK's performance in capturing sea level variability at different temporal scales

The SLA from XTRACK and TG are first decomposed into NLT, annual (seasonal), and residual signals, filtered using the DSR algorithm, and then compared. NLT includes low-frequency signals such as interannual variability and linear trend; the residual signal captures monthly to interannual signals; and the annual signal represents the seasonal variability in sea level. The analysis is conducted at 264 stations along the global coastline for the period 1994–2023.

https://doi.org/10.5194/egusphere-2026-4902
Preprint. Discussion started: 27 August 2026

Approximately 88% of stations (232 stations) show strong correlation ($r \geq 0.7$) with TG for the NLT signal (Fig. 9(a)), and 66% (175 stations) exhibit an RMSE ≤ 20mm (Fig. 10(a)). The NLT signal is influenced by decadal and/or multi-decadal oscillations, such as the El Niño-Southern Oscillation (ENSO) and the North Atlantic Oscillation (NAO), as well as long-term barystatic sea level changes, steric changes, and variations in wind or ocean circulation. NLT signals generally exhibit a larger spatial extent. The effectiveness of DSR is particularly evident at stations along very narrow coasts like the Santa Monica station, located on the northwest America with a shelf-width of ~14 km. Since DSR selects observations within a 250 km SR, but only those within the shelf-break, observations as far as 200 km from the TG (along the shelf) are selected and are found to capture the NLT signal observed at the coast by the TG ($r = 0.97$ and RMSE =9.5 mm).

Approximately 67% of stations (176 stations) show good correlation with TG for the residual signal (Fig. 9(b)), and only 21% exhibit a low RMSE (Fig. 10(b)). Residual signals arise from various sources of monthly to interannual sea level variability, such as those caused by coastal trapped waves (Chelton and Enfield, 1986; Wise et al., 2024). The DSR algorithm can capture residual signals in the coastal regions of western and southern Australia, northwest America, Long Island Sound, Baltic Sea, and North Sea. For example, at the Newport station in the Long Island Sound, we get $r = 0.83$ and RMSE = 16.6 mm. However, a clear contrast is evident between the coasts of eastern and western Australia. Along the east coast, the EAC generates numerous highly variable mesoscale eddies, which can interfere with coastal trapped waves near the shelf edge by influencing their energy flux and propagation characteristics (Freeland et al., 1986; Maiwa et al., 2010). Moreover, stations situated in tidally-dominated estuaries with high tides and turbidity, such as—Bay of Fundy and San Francisco Bay, show poor r and high RMSE. This poor residual signal correlation may arise from tidal influences often extending much farther upstream than saltwater intrusion in these estuaries, which in turn affects the ability of altimetry data to accurately capture the residual signal (Wells, 1995). In addition, stratification plays a significant role in the St. Lawrence Bay, which again can influence the propagation characteristics of internal waves (Saucier and Chassé, 2000) and hence we see poor r and RMSE.

About 97% of stations (257 stations) show a strong correlation between altimetry and TG at an annual scale (Fig. 9(c)). However, only 71% of the stations exhibit an RMSE ≤ 20mm (Fig. 10(c)). Variations in the annual signal are primarily driven by factors such as wind stress, sea surface temperature, and salinity changes (Abdallah and Eid, 1989). The Rimouski station located in the St. Lawrence Bay and the Anchorage station in the Turnagain Arm show poor correlations with the TG data—these stations are situated in highly turbid zones.

We also show, in Fig. C1 in Appendix C, the uncertainty in r at each station estimated using the Fisher Z-transformation. Finally, we assess the bias between TG and altimetry-derived SLA using stations referenced to the ellipsoid. A Student's *t*-test is applied to evaluate whether the bias is statistically significant. We found no significant bias (p-value>0.05). Fig. A1-A2 in Appendix A shows assessment of XTRACK's performance in capturing sea level variability across different temporal scales with TG linked to ellipsoid.

https://doi.org/10.5194/egusphere-2026-4902
Preprint. Discussion started: 27 August 2026

We also evaluate high frequency TG SLA data by comparing the TG observation closest in time to the satellite overpass containing that altimetry observation point (see S1 and Fig. S1 in Supplement).

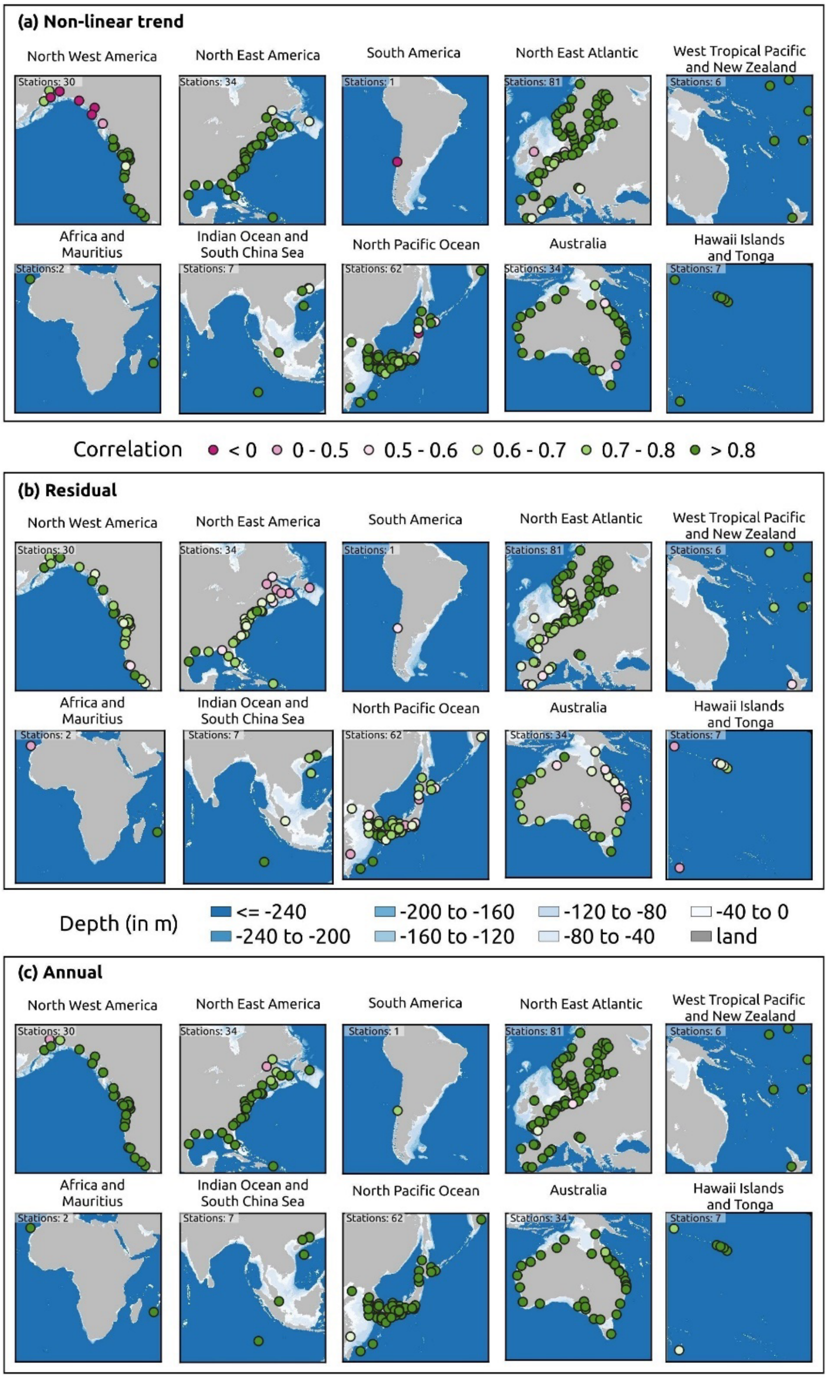

https://doi.org/10.5194/egusphere-2026-4902
Preprint. Discussion started: 27 August 2026

Figure 9 Assessment of XTRACK's performance in capturing sea level variability across different temporal scales: Correlation of XTRACK SLA with TG for (a) NLT, (b) residual signal, and (c) annual signal. Green shades indicate a strong correlation (r), while pink shades represent a weak correlation.

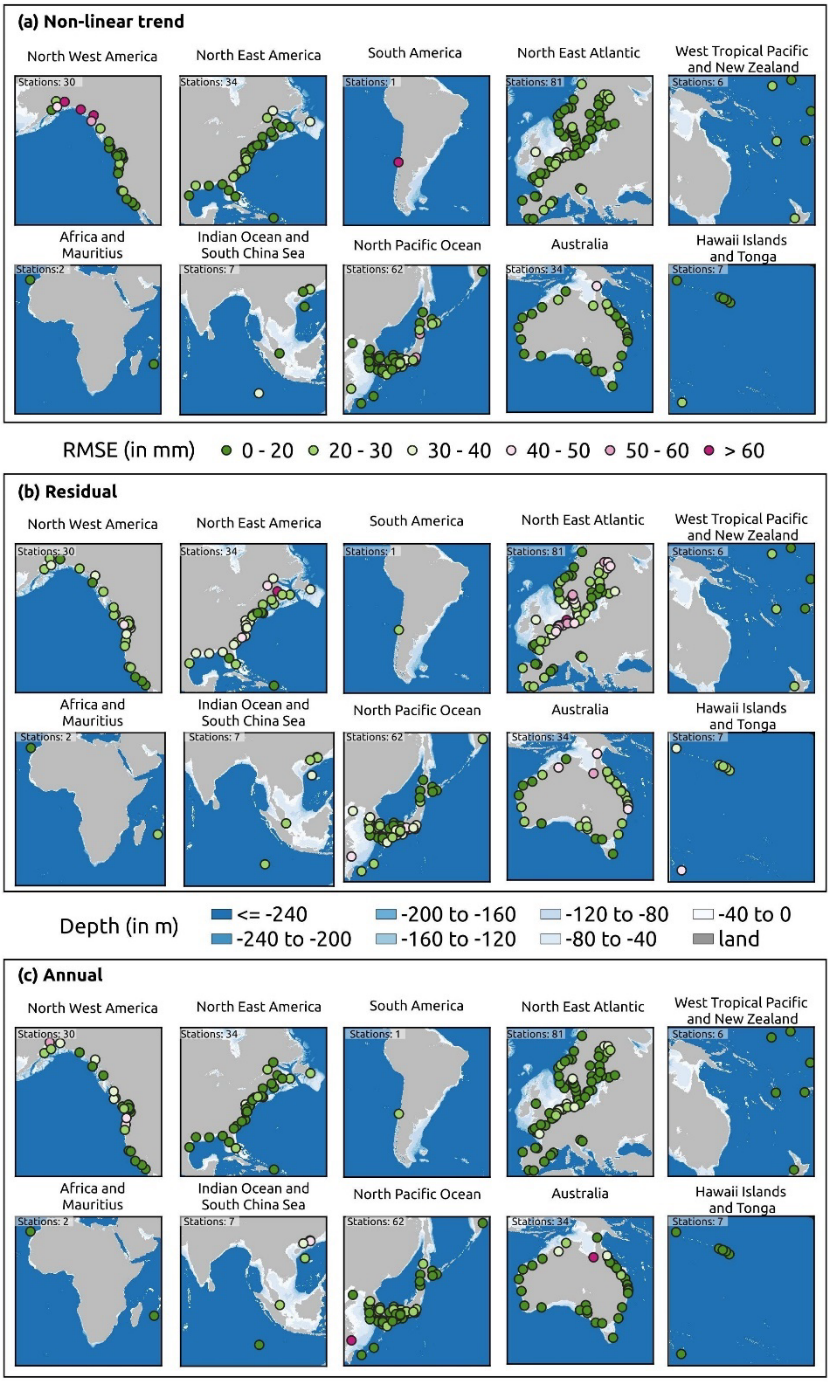

https://doi.org/10.5194/egusphere-2026-4902
Preprint. Discussion started: 27 August 2026

Figure 10 Assessment of XTRACK's performance in capturing sea level variability across different temporal scales: RMSE of XTRACK SLA with TG for (a) NLT, (b) residual signal, and (c) annual signal. Green shades indicate low RMSE, while pink shades represent high RMSE.

4.4 Coastal Sea Level Trends (CSLT)

CSLT over a 30-year period (1994–2023), is estimated at 248 stations (Fig. 11). Trends estimated from TG are highest at Uragami, Japan with 8.8±0.76 mm/yr, while the DSR-based altimetry trend is 4.62±0.86 mm/yr. The highest altimetry-based trend is observed at Onisaki, Japan (7.35±0.82 mm/yr), where the TG-based trend is 5.37±0.79 mm/yr.

The coastal sea level rise is most pronounced in Gulf of Mexico, Baltic Sea, several stations in Japan, and low-latitude northeast America. In the Baltic Sea, the mean trend is 4.24 ±1.37 mm/yr from TG and 4.62±1.3 mm/yr from altimetry. Similarly, Gulf of Mexico exhibits 5.2±0.67 mm/yr from TG and 5.09±0.57 mm/yr from altimetry. In contrast, CSLT trends are much lower in northwest America (1.82±0.62 mm/yr from TG and 1.74±0.59 mm/yr from altimetry). Earlier, Bonaduce et al. (2016) reported spatial variability in altimetry trends (mm/yr) across the Mediterranean Sea (Med Sea) (1993–2012), with slightly higher values at locations such as Trieste (TG: 3.19, altimetry: 3.1). Using a longer time series, we find lower trends (TG: 1.93 ± 0.56, altimetry: 2.5 ± 0.55), suggesting that the higher values in the shorter record were possibly influenced by interannual variability.

In general, trends from altimetry (X_DSR) fall within the uncertainty limits of the TG estimates at about 72% of stations (178 stations) (CSLT trend uncertainties at 95% confidence level from XTRACK and TG are shown in Fig. C2 in Appendix C). A paired *t*-test shows no statistically significant difference between TG and DSR-derived altimetry sea level trends ($t = -1.75$, $p = 0.08$, 95% confidence interval: [−0.34, 0.02]), suggesting that the two datasets are in good agreement. We find altimetry trends from X_DSR outside the uncertainty limits of TG trend estimates at 70 stations. Trends at 7 of these stations improved after TG stations were linked to the ellipsoid (see Fig. A3 in Appendix A, Fig. C3 in Appendix C, and Table S3 in Supplement). For example, the TG trend, referenced to Tide Gauge Benchmark (TGBM), at Onisaki is 5.37±0.79 mm/yr and from X_DSR is 7.35±0.82 mm/yr. After linking to the ellipsoid, the TG trend is 7.12±0.79 mm/yr, closely matching the X_DSR trend. Unfortunately, only 16 of the 70 TG stations have ellipsoidal links.

A full station list with trends from TG and XTRACK, along with uncertainties, is given in Table S2 in Supplement.

https://doi.org/10.5194/egusphere-2026-4902
Preprint. Discussion started: 27 August 2026

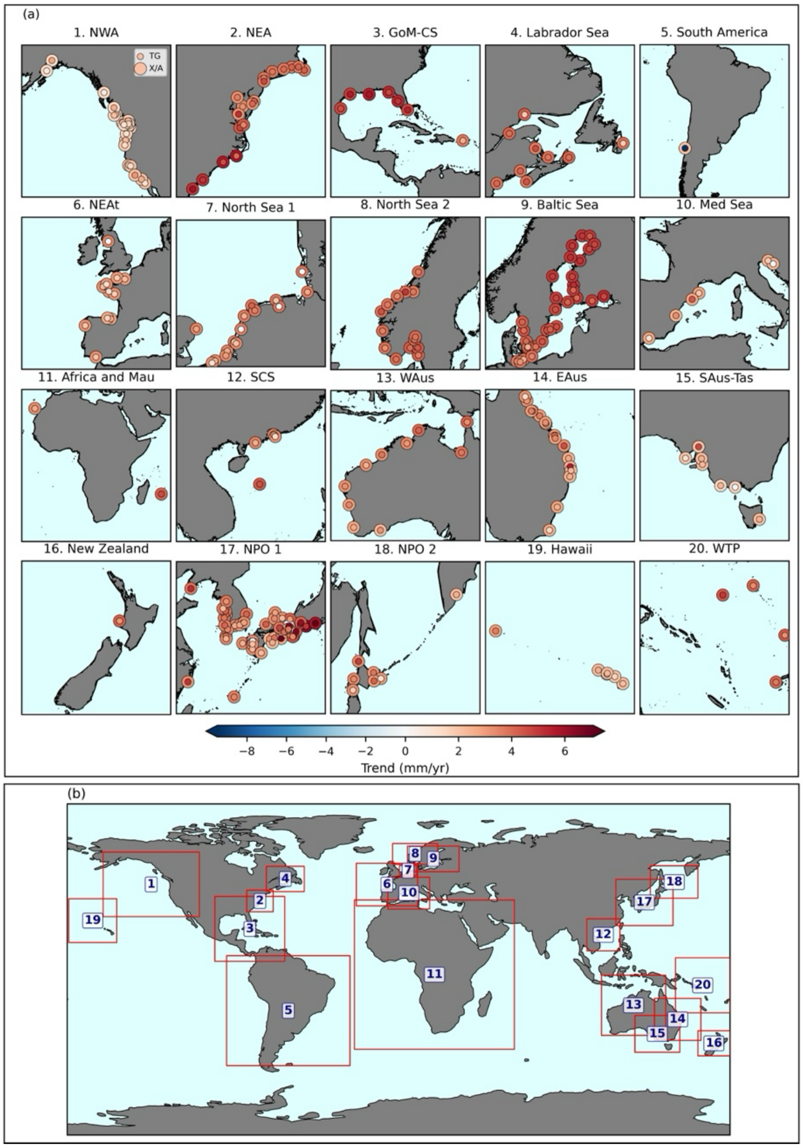

Figure 11 CSLT from 1994 to 2023 (30 years) derived from TG and coastal altimetry: Smaller circles represent trends from TG, and larger circles show trends from X_DSR. The colors indicate CSLT in mm/year, with red shades representing increasing trends and blue shades indicating decreasing trends. (a) Panels 1-20 shows region-wise SLA trends from TG and X_DSR and (b) shows world map and bounding boxes of region with box number corresponding to panel number. (c) shows the bounding boxes for the regions considered for the study. Regional abbreviations: NWA- northwest America, NEA- northeast America, GoM-CS- Gulf of Mexico – Caribbean Sea, NEAt- northeast Atlantic Ocean, Med Sea- Mediterranean Sea, Africa and Mau- Africa and Mauritius, SCS- South China Sea, WAus- western Australia, EAus- eastern Australia, Saus-Tas- southern Australia – Tasmania, NPO1- north Pacific Ocean 1, NPO2- north Pacific Ocean 2, WTP- west tropical Pacific Ocean.

https://doi.org/10.5194/egusphere-2026-4902
Preprint. Discussion started: 27 August 2026

5. Conclusions

The coastal sea level dynamics differ from the open ocean, primarily because ocean currents must flow parallel to the coastline (Hughes et al., 2019)—the biggest influences being coastal trapped waves and bottom effects (Hughes et al., 2019). Consequently, a novel altimetry data selection algorithm, called Dynamic Search Radius (DSR) is developed that chooses along-coast observations rather than open ocean points. The primary limitation of altimetry for coastal sea level monitoring lies in its temporal and spatial sampling. Temporal sampling is improved by incorporating observations from multiple satellite passes, ensuring at least 15 per month. We found that restricting observations to within the continental shelf significantly improves the representation of coastal sea level variability across multiple temporal scales, such as low-frequency—NLT (88% of stations have $r \geq 0.7$), seasonal—annual (97%), and monthly-to-interannual—residual (67%). The DSR algorithm consistently outperformed other altimetry selection algorithms, with the best performance observed across most regions, particularly in northeast America, northeast Atlantic Ocean, north Pacific Ocean, Indian Ocean – South China Sea, western Australia and New Zealand. We found that XTRACK/ALES provides limited improvement over XTRACK in capturing coastal sea level variability; however, both struggled at some stations in tidally dominated estuaries, Gulf of St. Lawrence, and along eastern Australia. Trend estimates for over a period of 30-years showed altimetry trends well within the uncertainty limits of TG trends, with the highest CSLT observed in the Gulf of Mexico (5.09±0.57 mm/yr), the Baltic Sea (4.62±1.3 mm/yr) and several stations in Japan and low-latitude northeast Atlantic. This work emphasizes that using DSR algorithm, altimetry is able to capture coastal sea level variability effectively at monthly and longer temporal scales. Furthermore, the study demonstrates that the lower-resolution product (XTRACK) can be reliable in capturing SLA signals at these time scales.

https://doi.org/10.5194/egusphere-2026-4902
Preprint. Discussion started: 27 August 2026

531 **Appendix A: Assessment of dynamic search radius (DSR) algorithm with tide gauges (TG) linked to ellipsoid.**

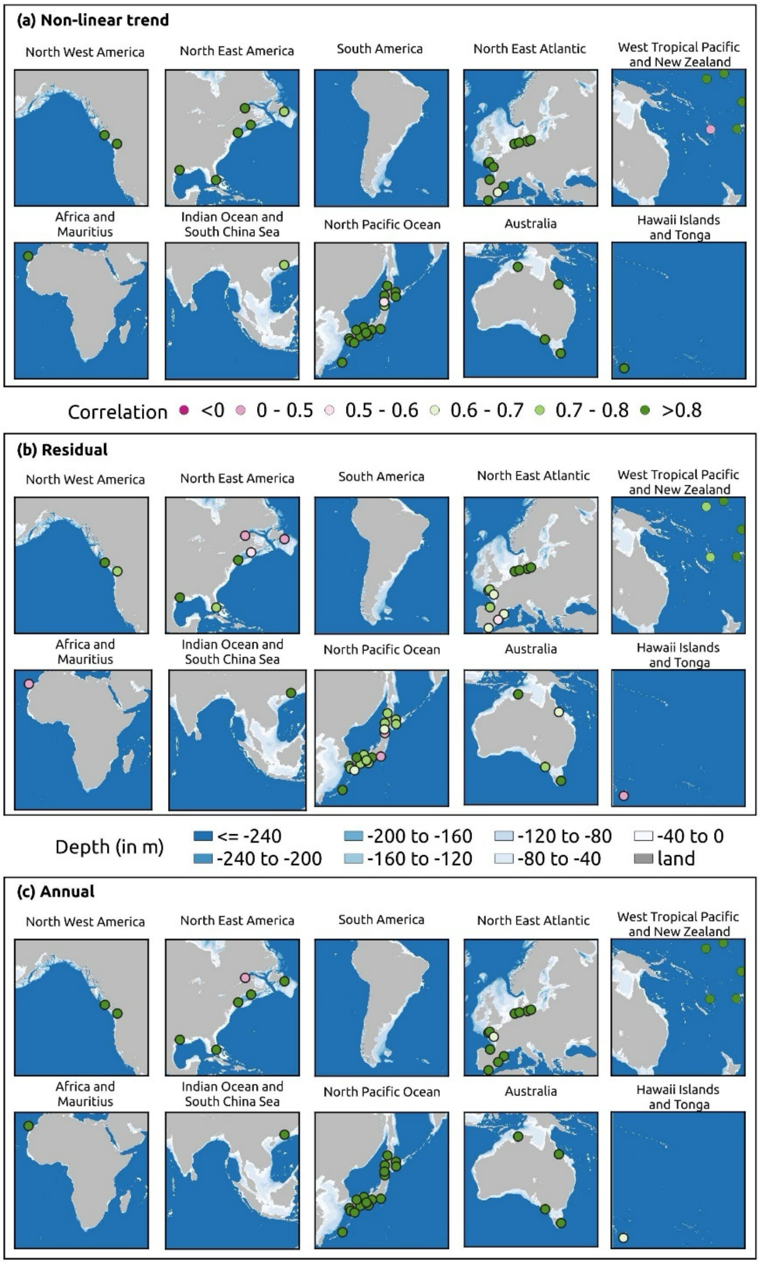

532

533 **Figure A1** Assessment of XTRACK's performance in capturing sea level variability across different temporal scales with tide
534 gauges (TG) linked to ellipsoid. Correlation for (a) non-linear trend, (b) residual signal, and (c) annual signal. Green shades
535 indicate a strong correlation (R), while pink shades represent a weak correlation.

https://doi.org/10.5194/egusphere-2026-4902
Preprint. Discussion started: 27 August 2026

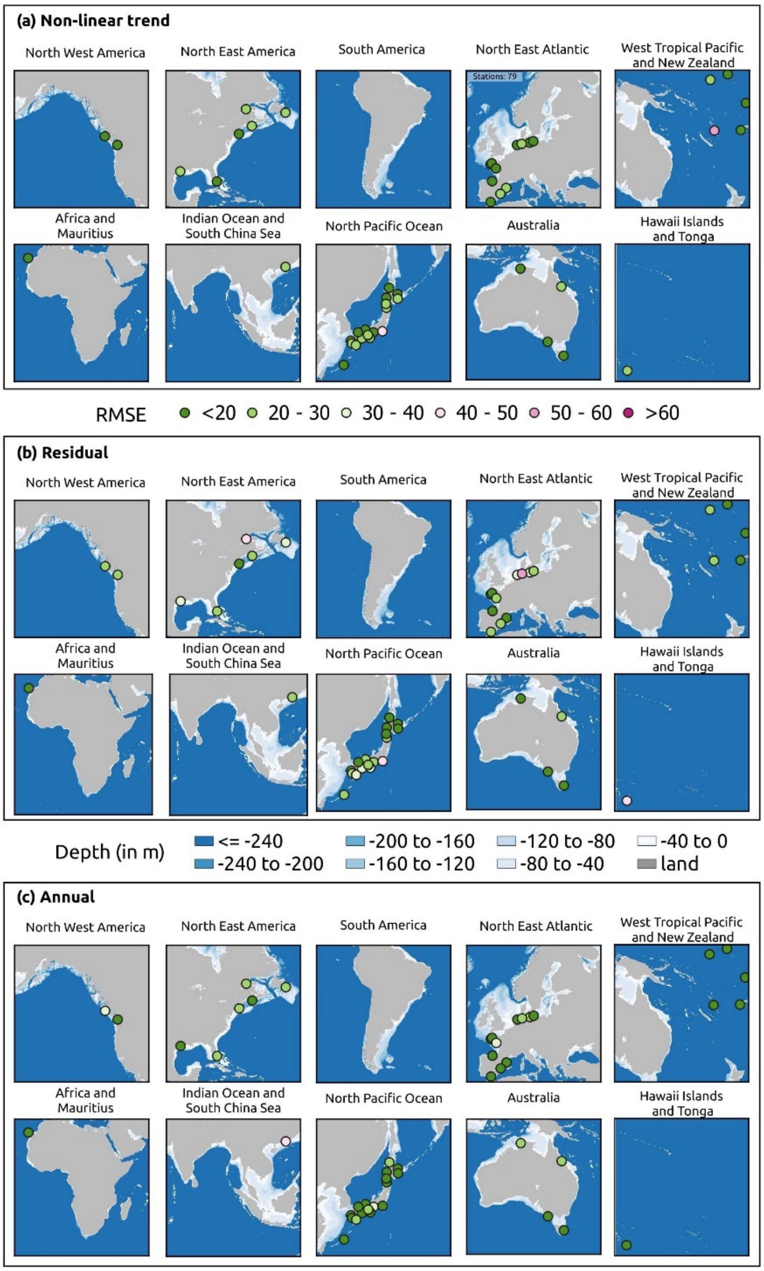

Figure A2 Assessment of XTRACK's performance in capturing sea level variability across different temporal scales with tide gauges (TG) linked to ellipsoid. RMSE for (a) non-linear trend, (b) residual signal, and (c) annual signal. Green shades indicate a low RMSE, while pink shades represent a high RMSE.

https://doi.org/10.5194/egusphere-2026-4902
Preprint. Discussion started: 27 August 2026

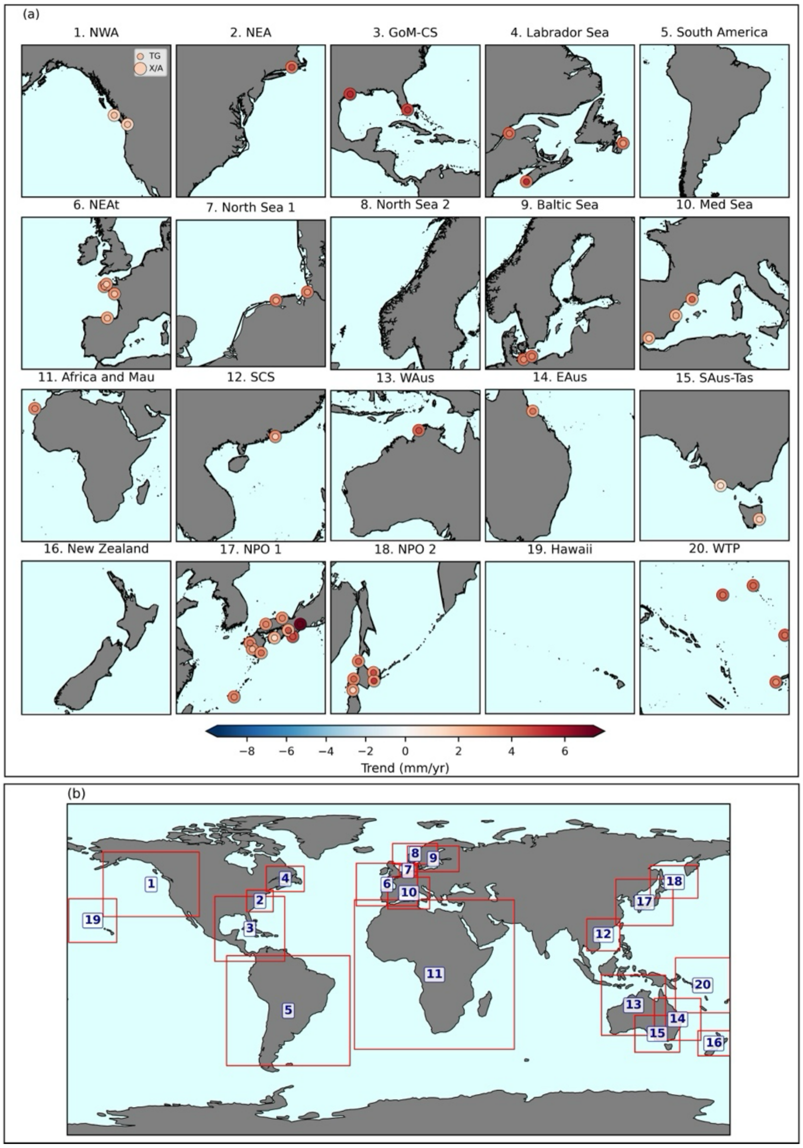

Figure A3 CSLT from 1994 to 2023 (30 years) derived from TG linked to ellipsoid and coastal altimetry: Smaller circles represent trends from TG, and larger circles show trends from X_DSR. The colors indicate CSLT in mm/year, with red shades representing increasing trends and blue shades indicating decreasing trends. (a) Panels 1-20 shows region-wise SLA trends from TG and X_DSR and (b) shows world map and bounding boxes of region with box number corresponding to panel number. (c) shows the bounding boxes for the regions considered for the study. Regional abbreviations: NWA- northwest America, NEA- northeast America, GoM-CS- Gulf of Mexico – Caribbean Sea, NEAt- northeast Atlantic Ocean, Med Sea- Mediterranean Sea, Africa and Mau- Africa and Mauritius, SCS- South China Sea, WAus- western Australia, EAus- eastern

https://doi.org/10.5194/egusphere-2026-4902
Preprint. Discussion started: 27 August 2026

Australia, Saus-Tas- southern Australia – Tasmania, NPO1- north Pacific Ocean 1, NPO2- north Pacific Ocean 2, WTP- west tropical Pacific Ocean.

Appendix B: Sensitivity to parameter choice.

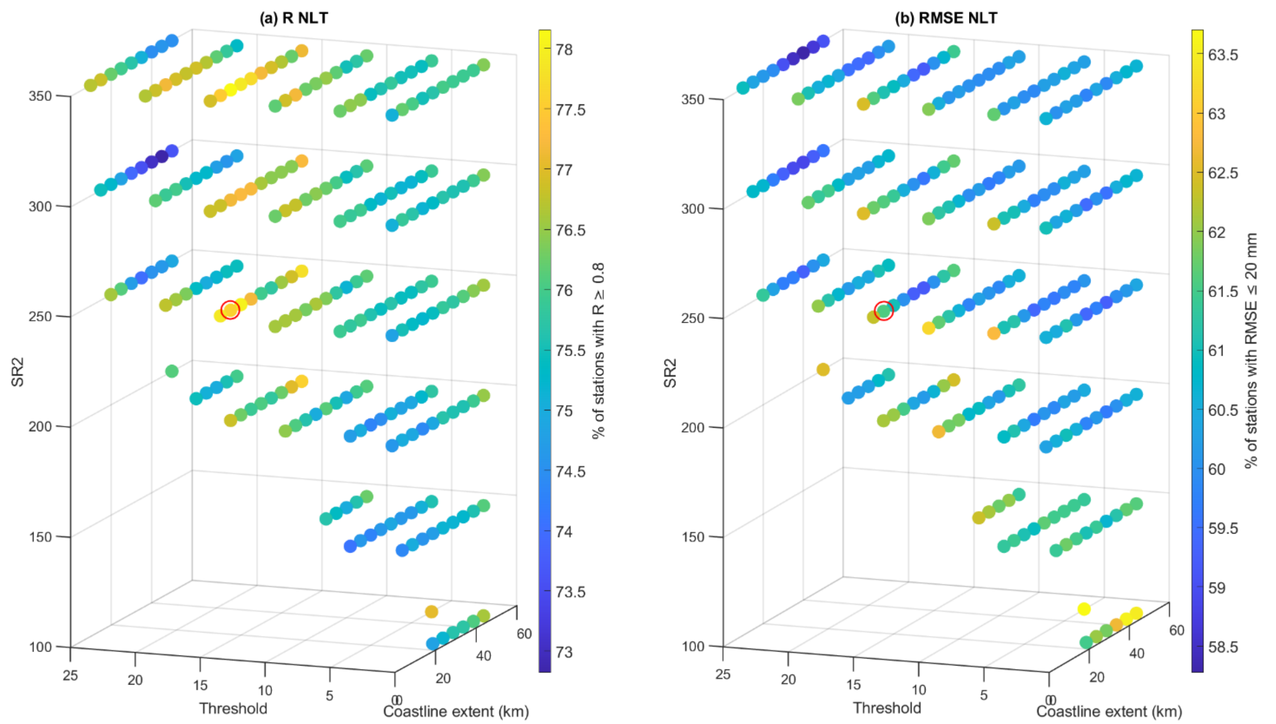

Figure B1 Three-dimensional scatter plots illustrating the sensitivity analysis across 242 parameter combinations of threshold, coastline extent, and SR2, based on 312 TG stations for NLT signal. The x-axis represents coastline extent (in km), the y-axis shows threshold, and the z-axis corresponds to SR2 (in km). The colour of each circle in (a) denotes the percentage of stations with r ≥ 0.8 for Non-Linear Trend signal (R_NLT) and in (b) denotes the percentage of stations with RMSE ≤ 20 mm for Non-Linear Trend signal (RMSE_NLT). A red circle highlights the optimal parameter combination (15, 15, 250), identified as the best among 396 initial configurations. Only 242 combinations are shown, as combinations resulting in the exclusion of more than 15% of total stations were removed. The color scale spans a narrow range, from 72% - 78% of stations achieving r ≥ 0.8 (explaining at least 64% of the in-situ observed (TG) variability in non-linear trend signal of the coastal sea level anomaly) and 53% - 68% of stations meeting the RMSE criterion. Note that after filtering, 6 combinations remained, with coastline extents of 10, 15 and 20, thresholds of 15, and 20, and SR2 values of 200, 250 and 350.

https://doi.org/10.5194/egusphere-2026-4902
Preprint. Discussion started: 27 August 2026

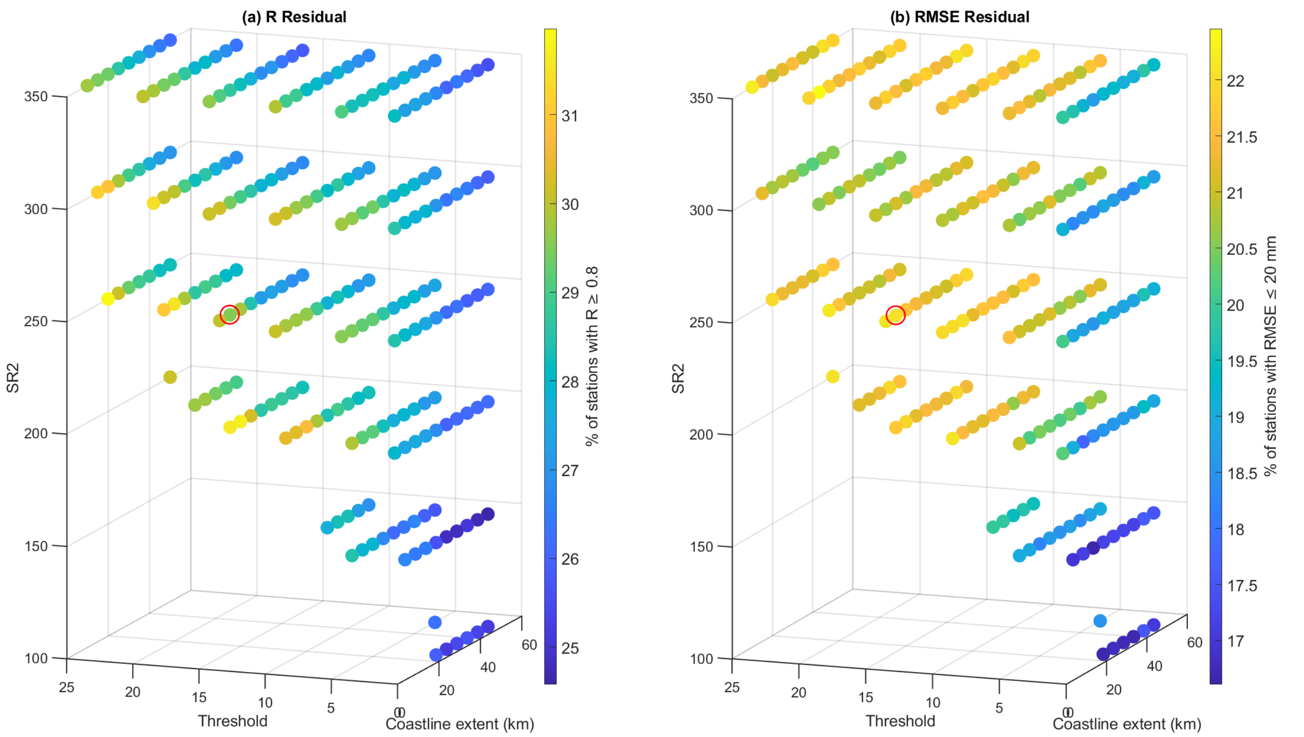

Figure B2 Three-dimensional scatter plots illustrating the sensitivity analysis across 242 parameter combinations of threshold, coastline extent, and SR2, based on 312 TG stations for residual signal. The x-axis represents coastline extent (in km), the y-axis shows threshold, and the z-axis corresponds to SR2 (in km). The colour of each circle in (a) denotes the percentage of stations with r ≥ 0.8 for residual signal (R_Residual) and in (b) denotes the percentage of stations with RMSE ≤ 20 mm for residual signal (RMSE_Residual). A red circle highlights the optimal parameter combination (15, 15, 250), identified as the best among 396 initial configurations. Only 242 combinations are shown, as combinations resulting in the exclusion of more than 15% of total stations were removed. The color scale spans a narrow range, from 24% - 32% of stations achieving r ≥ 0.8 (explaining at least 64% of the in-situ observed (TG) variability in residual signal of the coastal sea level anomaly) and 15% - 24% of stations meeting the RMSE criterion. Note that after filtering, 6 combinations remained, with coastline extents of 10, 15 and 20, thresholds of 15, and 20, and SR2 values of 200, 250 and 350.

https://doi.org/10.5194/egusphere-2026-4902
Preprint. Discussion started: 27 August 2026

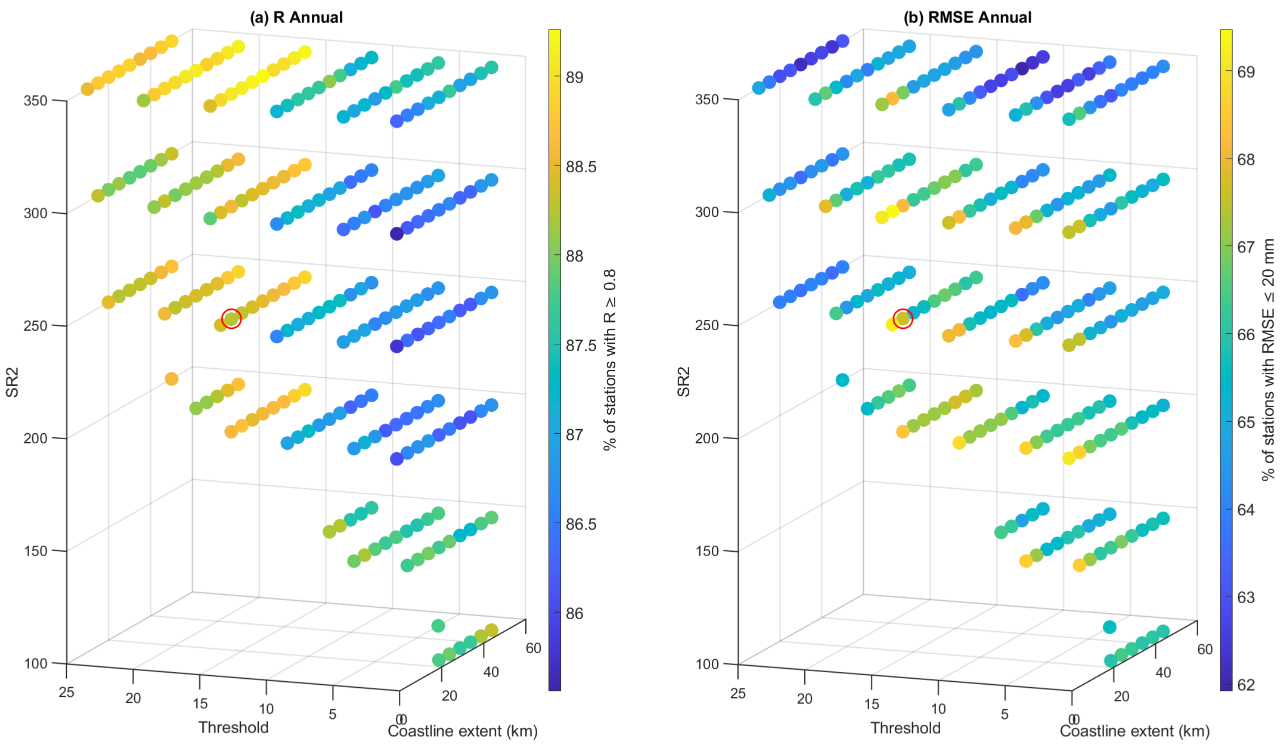

Figure B3 Three-dimensional scatter plots illustrating the sensitivity analysis across 242 parameter combinations of threshold, coastline extent, and SR2, based on 312 TG stations for annual signal. The x-axis represents coastline extent (in km), the y-axis shows threshold, and the z-axis corresponds to SR2 (in km). The colour of each circle in (a) denotes the percentage of stations with $r \geq 0.8$ for annual signal (R_Annual) and in (b) denotes the percentage of stations with RMSE ≤ 20 mm for annual signal (RMSE_Annual). A red circle highlights the optimal parameter combination (15, 15, 250), identified as the best among 396 initial configurations. Only 242 combinations are shown, as combinations resulting in the exclusion of more than 10% of total stations were removed. The color scale spans a wide range, from 76% - 100% of stations achieving $r \geq 0.8$ (explaining at least 64% of the in-situ observed (TG) variability in annual signal of the coastal sea level anomaly) and 58% - 73% of stations meeting the RMSE criterion. Note that after filtering, 6 combinations remained, with coastline extents of 10, 15 and 20, thresholds of 15, and 20, and SR2 values of 200, 250 and 350.

Table B1 The six parameter combinations remaining after filtering the 396 combinations, based on performance. Please note that the performance metrics used are the percentage of stations discarded for not meeting DSR algorithm's requirements, percentage of stations with $r \geq 0.8$ and the percentage of stations with RMSE ≤ 20 mm.

Sl. No.	Coastline Extent	Threshold	SR2
1	10 km	15	250 km

https://doi.org/10.5194/egusphere-2026-4902
Preprint. Discussion started: 27 August 2026

2	10 km	20	350 km
3	15 km	15	200 km
4	15 km	15	250 km
5	15 km	20	250 km
6	20 km	15	200 km

https://doi.org/10.5194/egusphere-2026-4902
Preprint. Discussion started: 27 August 2026

Appendix C: Estimates of uncertainties.

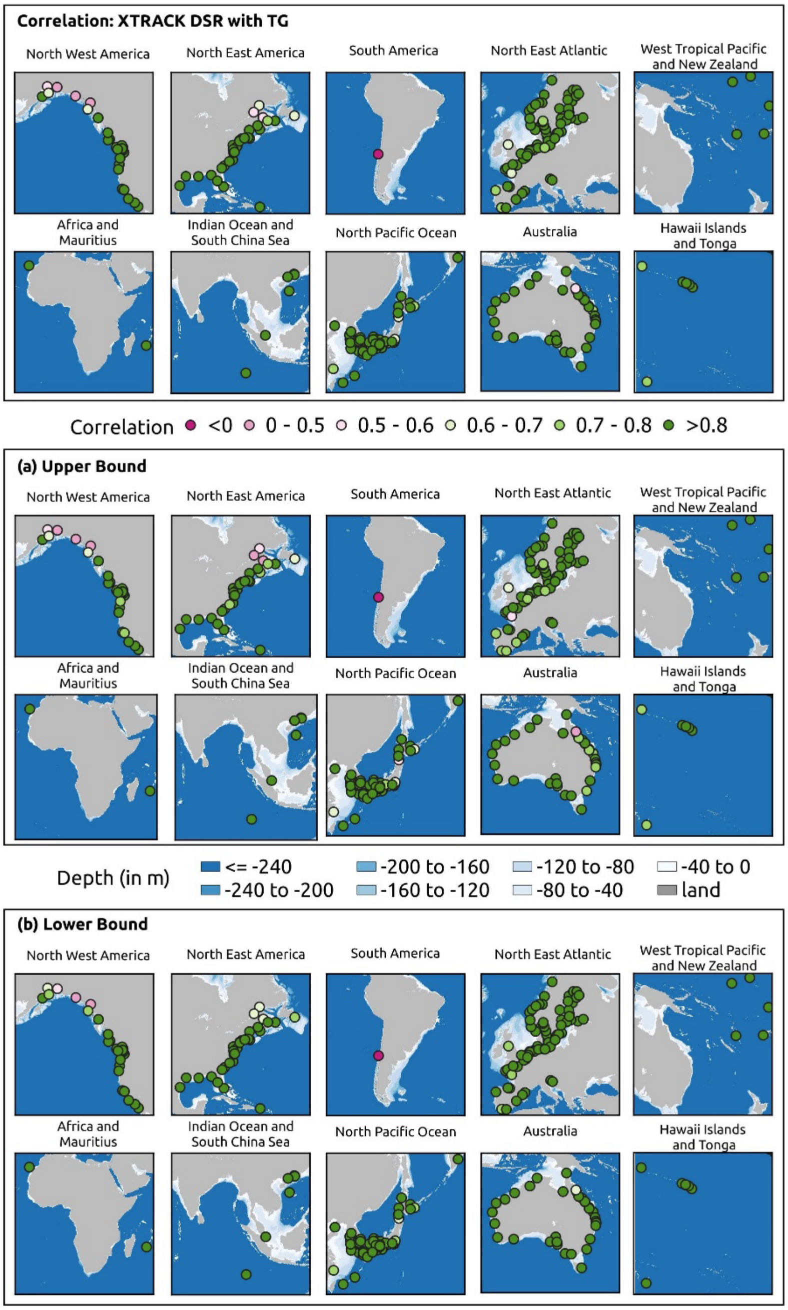

Figure C1 Results from uncertainty in correlation coefficient at each station estimated using the Fisher Z-transformation. (a) upper bound of correlation coefficient of SLA from X_DSR and TG, (b) lower bound of SLA from X_DSR and TG.

https://doi.org/10.5194/egusphere-2026-4902
Preprint. Discussion started: 27 August 2026

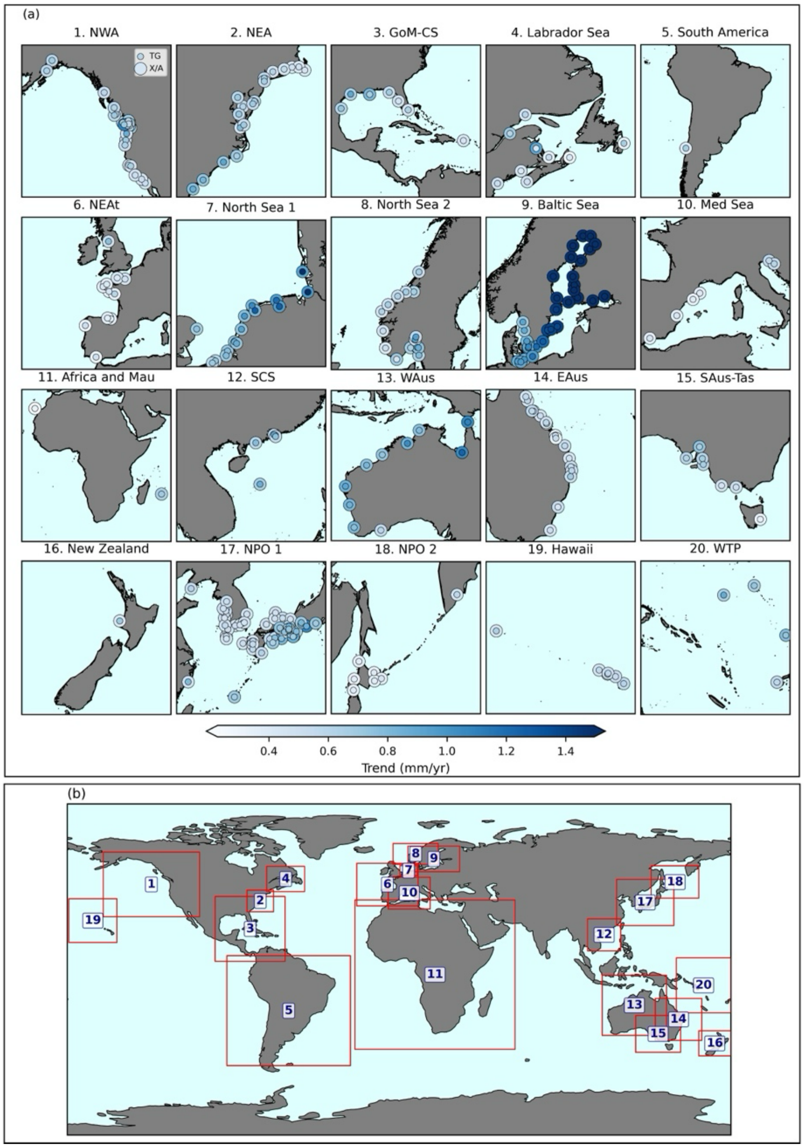

Figure C2 Trend uncertainties of coastal sea level from TG and altimetry (X_DSR) at 95% confidence level. Smaller circles represent trend uncertainties from TG and larger circles show uncertainties from XTRACK (DSR algorithm). The colors indicate the magnitude of trend uncertainties in mm/year. (a) Panels 1-20 shows region-wise uncertainties in SLA trends from TG and X_DSR and (b) shows world map and bounding boxes of the regions with box number corresponding to panel number. Regional abbreviations: NWA- northwest America, NEA- northeast America, GoM-CS- Gulf of Mexico – Caribbean Sea, NEAt- northeast Atlantic Ocean, Med Sea- Mediterranean Sea, Africa and Mau- Africa and Mauritius, SCS- South China Sea, WAus- western Australia, EAus- eastern Australia, Saus-Tas- southern Australia – Tasmania, NPO1- north Pacific Ocean 1, NPO2- north Pacific Ocean 2, WTP- west tropical Pacific Ocean.

https://doi.org/10.5194/egusphere-2026-4902
Preprint. Discussion started: 27 August 2026

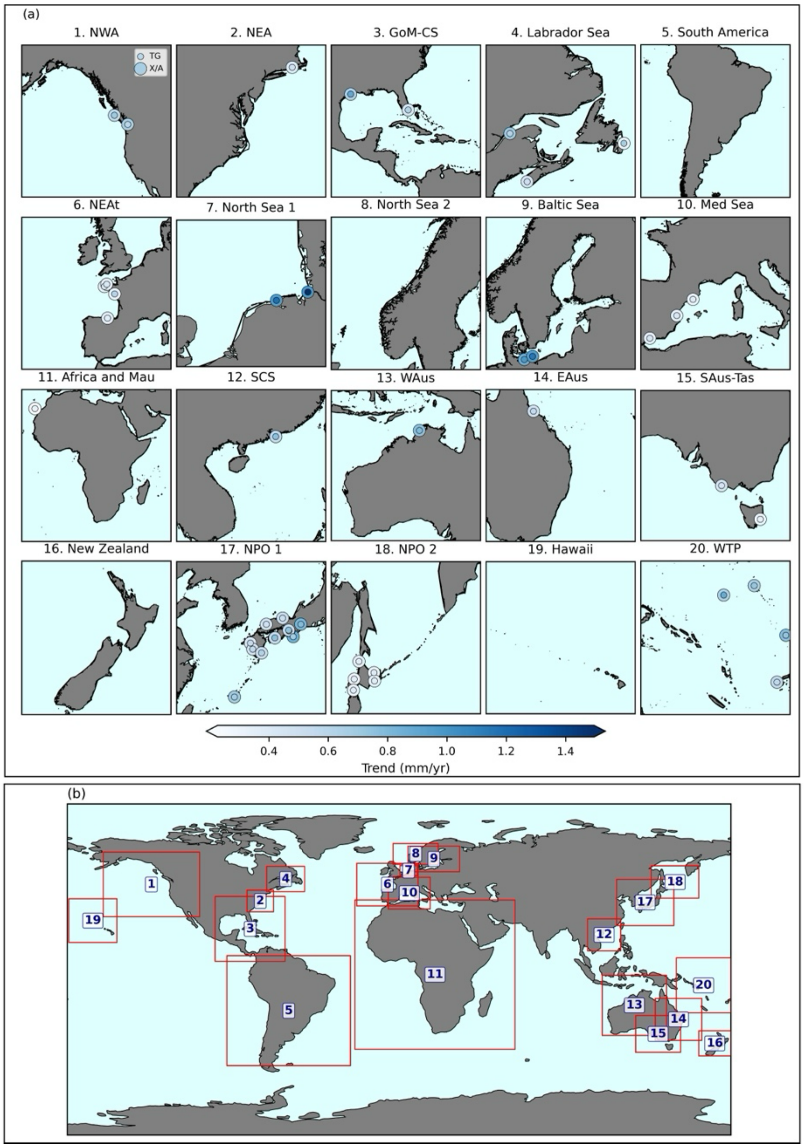

Figure C3 Trend uncertainties of coastal sea level from TG linked to ellipsoid and altimetry (X_DSR) at 95% confidence level. Smaller circles represent trend uncertainties from TG and larger circles show uncertainties from XTRACK (DSR algorithm). The colors indicate the magnitude of trend uncertainties in mm/year. (a) Panels 1-20 shows region-wise uncertainties in SLA trends from TG linked to ellipsoid and X_DSR and (b) shows world map and bounding boxes of the regions with box number corresponding to panel number. Regional abbreviations: NWA- northwest America, NEA- northeast America, GoM-CS- Gulf of Mexico – Caribbean Sea, NEAt- northeast Atlantic Ocean, Med Sea- Mediterranean Sea, Africa and Mau- Africa and Mauritius, SCS- South China Sea, WAus- western Australia, EAus- eastern Australia, Saus-Tas- southern Australia – Tasmania, NPO1- north Pacific Ocean 1, NPO2- north Pacific Ocean 2, WTP- west tropical Pacific Ocean.

Data availability

All data used are open source and are available at: in-situ tide gauge data from PSMSL (https://psmsl.org/), X-TRACK SLA L2P v2.2 (referred to as XTRACK) from AVISO website (https://www.aviso.altimetry.fr/en/data/products/sea-surface-height-products/regional/x-track-sla/x-track-l2p-sla-version-2022.html) and Along-track sea level anomalies and trends v3.0 (2025) (referred to as XTRACK/ALES) from SEANOE website (https://www.seanoe.org/data/00631/74354/), Dynamic Atmospheric Correction (DAC) using ERA5 data distributed freely by AVISO (https://www.aviso.altimetry.fr/en/data/products/auxiliary-products/dynamic-atmospheric-correction.html), Vertical Land Motion (VLM) rates at PSMSL stations from GPS network produced and distributed freely by Nevada Geodetic Laboratory (NGL) (https://geodesy.unr.edu/vlm.php) and, GEBCO_2025, a gridded global bathymetry dataset (https://www.gebco.net/data-products-gridded-bathymetry-data/gebco2025-grid)

Code availability

The original codes of DSR algorithm are available at https://github.com/Vandana1195/Dynamic-Search-Radius. All processed data required to run the code are available on Zenodo at https://doi.org/10.5281/zenodo.17367435

Author contributions

VS and BDV, Conceptualization and methodology; VS, Formal analysis; VS and BDV, Investigation; BDV, Resources; VS, Data curation; VS and BDV, Writing – original draft; VS and BDV, Writing – review & editing.

Competing interests

The contact author has declared that none of the authors has any competing interests.

Disclaimer

Publisher's note: Copernicus Publications remains neutral with regard to jurisdictional claims made in the text, published maps, institutional affiliations, or any other geographical representation in this paper. The authors bear the ultimate responsibility for providing appropriate place names. Views expressed in the text are those of the authors and do not necessarily reflect the views of the publisher.

Acknowledgements

VS acknowledges the Ministry of Education for the PhD fellowship. VS and BDV express their gratitude to Diljit Dutta for discussions and his insightful comments.

Financial support

The authors acknowledge financial support from Anusandhan National Research Foundation (ANRF) (previously known as Science and Engineering Research Board (SERB)) under the grant agreement SRG/2022/000625.

References

Abdallah, A. M. and Eid, F. M.: On the steric sea level in the Red Sea, The International Hydrographic Review, 1989.

Abele, A., Royston, S., and Bamber, J.: The Impact of Altimetry Corrections of Sentinel-3A Sea Surface Height in the Coastal Zone of the Northwest Atlantic, Remote Sens. (Basel)., 15, 1132, 2023.

Akpinar, A., Sadighrad, E., Fach, B. A., and Arkin, S.: Eddy Induced Cross-Shelf Exchanges in the Black Sea, Remote Sens. (Basel)., 14, https://doi.org/10.3390/rs14194881, 2022.

Allen, S. E.: Restrictions on deep flow across the shelf-break and the role of submarine canyons in facilitating such flow, Surv. Geophys., 25, 221–247, https://doi.org/10.1007/s10712-004-1275-0, 2004.

Benveniste, J., Birol, F., Calafat, F., Cazenave, A., Dieng, H., Gouzenes, Y., Legeais, J. F., Léger, F., Niño, F., Passaro, M., Schwatke, C., Shaw, A., and Team, T. C. C. I. C. S. L.: Coastal sea level anomalies and associated trends from Jason satellite altimetry over 2002–2018, Sci. Data, 7, 357, https://doi.org/10.1038/s41597-020-00694-w, 2020.

Bhowmik, R. Das and Sankarasubramanian, A.: Limitations of univariate linear bias correction in yielding cross-correlation between monthly precipitation and temperature, International Journal of Climatology, 39, 4479–4496, 2019.

Birol, F., Fuller, N., Lyard, F., Cancet, M., Niño, F., Delebecque, C., Fleury, S., Toublanc, F., Melet, A., Saraceno, M., and Léger, F.: Coastal applications from nadir altimetry: Example of the X-TRACK regional products, Advances in Space Research, 59, 936–953, https://doi.org/10.1016/j.asr.2016.11.005, 2017.

Birol, F., Léger, F., Passaro, M., Cazenave, A., Niño, F., Calafat, F. M., Shaw, A., Legeais, J. F., Gouzenes, Y., Schwatke, C., and Benveniste, J.: The X-TRACK/ALES multi-mission processing system: New advances in altimetry towards the coast, Advances in Space Research, 67, 2398–2415, https://doi.org/10.1016/j.asr.2021.01.049, 2021.

Blewitt, G., Kreemer, C., Hammond, W. C., and Gazeaux, J.: MIDAS robust trend estimator for accurate GPS station velocities without step detection, J. Geophys. Res. Solid Earth, 121, 2054–2068, https://doi.org/10.1002/2015JB012552, 2016.

Bonaduce, A., Pinardi, N., Oddo, P., Spada, G., and Larnicol, G.: Sea-level variability in the Mediterranean Sea from altimetry and tide gauges, Clim. Dyn., 47, 2851–2866, 2016.

Camargo, C. M. L., Piecuch, C. G., and Raubenheimer, B.: From Shelfbreak to Shoreline: Coastal sea level and local ocean dynamics in the Northwest Atlantic, Geophys. Res. Lett., 51, e2024GL109583, 2024.

Cazenave, A., Gouzenes, Y., Birol, F., Leger, F., Passaro, M., Calafat, F. M., Shaw, A., Nino, F., Legeais, J. F., Oelsmann, J., Restano, M., and Benveniste, J.: Sea level along the world's coastlines can be measured by a network of virtual altimetry stations, Commun. Earth Environ., 3, https://doi.org/10.1038/s43247-022-00448-z, 2022.

Cazenave, A., Gouzenes, Y., Leclercq, L., Birol, F., Legér, F., Passaro, M., Calafat, F. M., Shaw, A., Niño, F., and Legeais, J. F.: New network of virtual altimetry stations for measuring sea level along the world coastlines, New network of virtual altimetry stations for measuring sea level along the world coastlines, 2025.

Chelton, D. B. and Enfield, D. B.: Ocean signals in tide gauge records, J. Geophys. Res. Solid Earth, 91, 9081–9098, 1986.

Cleveland, R. B., Cleveland, W. S., McRae, J. E., and Terpenning, I.: STL: A seasonal-trend decomposition, J. off. Stat, 6, 3–73, 1990.

Deng, X. and Featherstone, W. E.: A coastal retracking system for satellite radar altimeter waveforms: Application to ERS-2 around Australia, J. Geophys. Res. Oceans, 111, 2006.

Dettmering, D., Müller, F. L., Oelsmann, J., Passaro, M., Schwatke, C., Restano, M., Benveniste, J., and Seitz, F.: NorthSEAL: A New Dataset of Sea Level Changes in the North Sea from Satellite Altimetry, Earth System Science Data Discussions, 2021, 1–28, 2021.

Dieng, H. B., Dadou, I., Léger, F., Morel, Y., Jouanno, J., Lyard, F., and Allain, D.: Sea level anomalies using altimetry, model and tide gauges along the African coasts in the Eastern Tropical Atlantic Ocean: Inter-comparison and temporal variability, Advances in Space Research, 68, 534–552, https://doi.org/10.1016/j.asr.2019.10.019, 2021.

Dinardo, S., Fenoglio-Marc, L., Buchhaupt, C., Becker, M., Scharroo, R., Fernandes, M. J., and Benveniste, J.: Coastal sar and plrm altimetry in german bight and west baltic sea, Advances in Space Research, 62, 1371–1404, 2018.

Dinardo, S., Fenoglio-Marc, L., Becker, M., Scharroo, R., Fernandes, M. J., Staneva, J., Grayek, S., and Benveniste, J.: A RIP-based SAR retracker and its application in North East Atlantic with Sentinel-3, Advances in Space Research, 68, 892–929, 2021.

Druon, J. N., Langlois, G., and Le Fèvre, J.: Simulating vertical mixing in a shelf-break region:: addition of a shear instability model, accounting for the overall effect of internal tides, on top of a one-dimensional turbulence closure mixed layer model, Cont. Shelf Res., 21, 423–454, https://doi.org/10.1016/S0278-4343(00)00090-X, 2001a.

Druon, J.-N., Langlois, G., and Le Fèvre, J.: Simulating vertical mixing in a shelf-break region: addition of a shear instability model, accounting for the overall effect of internal tides, on top of a one-dimensional turbulence closure mixed layer model, Cont. Shelf Res., 21, 423–454, 2001b.

Durrant, T. H., Greenslade, D. J. M., and Simmonds, I.: Validation of Jason-1 and Envisat Remotely Sensed Wave Heights, J. Atmos. Ocean. Technol., 26, 123–134, https://doi.org/10.1175/2008JTECHO598.1, 2009.

Emery, K. O. and Aubrey, D. G.: Sea levels, land levels, and tide gauges, Springer Science & Business Media, 2012.

https://doi.org/10.5194/egusphere-2026-4902
Preprint. Discussion started: 27 August 2026

Franco, B. C., Palma, E. D., Combes, V., and Lasta, M. L.: Physical processes controlling passive larval transport at the Patagonian Shelf Break Front, J. Sea Res., 124, 17–25, https://doi.org/10.1016/j.seares.2017.04.012, 2017.

Franco, B. C., Ruiz-Etcheverry, L. A., Marrari, M., Piola, A. R., and Matano, R. P.: Climate Change Impacts on the Patagonian Shelf Break Front, Geophys. Res. Lett., 49, https://doi.org/10.1029/2021GL096513, 2022.

Fratantoni, P. S. and Pickart, R. S.: Variability of the shelf break jet in the Middle Atlantic Bight: Internally or externally forced?, J. Geophys. Res. Oceans, 108, 2003.

Freeland, H. J., Boland, F. M., Church, J. A., Clarke, A. J., Forbes, A. M. G., Huyer, A., Smith, R. L., Thompson, R., and White, N. J.: The Australian Coastal Experiment: A search for coastal-trapped waves, J. Phys. Oceanogr., 16, 1230–1249, 1986.

Fu, L.-L. and Cazenave, A.: Satellite altimetry and earth sciences: a handbook of techniques and applications, Elsevier, 2000.

Gawarkiewicz, G. G., Todd, R. E., Plueddemann, A. J., Andres, M., and Manning, J. P.: Direct interaction between the Gulf Stream and the shelfbreak south of New England, Sci. Rep., 2, https://doi.org/10.1038/srep00553, 2012.

Gómez-Enri, J., Vignudelli, S., Quartly, G. D., Gommenginger, C. P., Cipollini, P., Challenor, P. G., and Benveniste, J.: Modeling Envisat RA-2 waveforms in the coastal zone: Case study of calm water contamination, IEEE Geoscience and Remote Sensing Letters, 7, 474–478, 2010.

Gomez-Enri, J., Cipollini, P., Passaro, M., Vignudelli, S., Tejedor, B., and Coca, J.: Coastal altimetry products in the strait of Gibraltar, IEEE Transactions on Geoscience and Remote Sensing, 54, 5455–5466, 2016.

Gouzenes, Y., Léger, F., Cazenave, A., Birol, F., Bonnefond, P., Passaro, M., Nino, F., Almar, R., Laurain, O., Schwatke, C., Legeais, J. F., and Benveniste, J.: Coastal sea level rise at senetosa (Corsica) during the jason altimetry missions, Ocean Science, 16, 1165–1182, https://doi.org/10.5194/os-16-1165-2020, 2020.

Graham, J. A., Rosser, J. P., O'Dea, E., and Hewitt, H. T.: Resolving Shelf Break Exchange Around the European Northwest Shelf, Geophys. Res. Lett., 45, 12386–12395, https://doi.org/10.1029/2018GL079399, 2018.

Hammond, W. C., Blewitt, G., and Kreemer, C.: GPS Imaging of vertical land motion in California and Nevada: Implications for Sierra Nevada uplift, J. Geophys. Res. Solid Earth, 121, 7681–7703, https://doi.org/10.1002/2016JB013458, 2016.

Hampel, F. R.: The influence curve and its role in robust estimation, J. Am. Stat. Assoc., 69, 383–393, 1974.

Hauer, M. E., Fussell, E., Mueller, V., Burkett, M., Call, M., Abel, K., McLeman, R., and Wrathall, D.: Sea-level rise and human migration, Nat. Rev. Earth Environ., 1, 28–39, 2020.

Heger, M. P. and Vashold, L.: Disappearing Coasts in the Maghreb: Coastal Erosion and Its Costs, World Bank Group: World Bank, the National Oceanographic Center (NOC) of the United Kingdom and the European Space Agency, 2021.

Hirzel, A. J., Alatalo, P., Oliver, H., Petitpas, C. M., Turner, J. T., Zhang, W. G., and McGillicuddy Jr, D. J.: High resolution analysis of plankton distributions at the middle atlantic bight shelf-break front, Cont. Shelf Res., 267, https://doi.org/10.1016/j.csr.2023.105113, 2023.

Hughes, C. W., Williams, J., Blaker, A., Coward, A., and Stepanov, V.: A window on the deep ocean: the special value of ocean bottom pressure for monitoring the large-scale, deep-ocean circulation, Prog. Oceanogr., 161, 19–46, 2018.

https://doi.org/10.5194/egusphere-2026-4902
Preprint. Discussion started: 27 August 2026

Hughes, C. W., Fukumori, I., Griffies, S. M., Huthnance, J. M., Minobe, S., Spence, P., Thompson, K. R., and Wise, A.: Sea level and the role of coastal trapped waves in mediating the influence of the open ocean on the coast, Surv. Geophys., 40, 1467–1492, 2019.

Huthnance, J. M.: On coastal trapped waves: Analysis and numerical calculation by inverse iteration, J. Phys. Oceanogr., 8, 74–92, 1978.

Johnson, E. E., Suanda, S. H., Wing, S. R., Currie, K. I., and Smith, R. O.: Episodic Summer Chlorophyll-a Blooms Driven by Along-Front Winds at Aotearoa's Southeast Shelf Break Front, J. Geophys. Res. Oceans, 128, e2022JC019609, 2023a.

Johnson, E. E., Suanda, S. H., Wing, S. R., Currie, K. I., and Smith, R. O.: Episodic Summer Chlorophyll-a Blooms Driven by Along-Front Winds at Aotearoa's Southeast Shelf Break Front, JOURNAL OF GEOPHYSICAL RESEARCH-OCEANS, 128, https://doi.org/10.1029/2022JC019609, 2023b.

Kummu, M., de Moel, H., Salvucci, G., Viviroli, D., Ward, P. J., and Varis, O.: Over the hills and further away from coast: global geospatial patterns of human and environment over the 20th–21st centuries, Environmental Research Letters, 11, 034010, https://doi.org/10.1088/1748-9326/11/3/034010, 2016.

Linder, C. A. and Gawarkiewicz, G.: A climatology of the shelfbreak front in the Middle Atlantic Bight, J. Geophys. Res. Oceans, 103, 18405–18423, 1998.

Maiwa, K., Masumoto, Y., and Yamagata, T.: Characteristics of coastal trapped waves along the southern and eastern coasts of Australia, J. Oceanogr., 66, 243–258, 2010.

Marti, F., Cazenave, A., Birol, F., Passaro, M., Léger, F., Niño, F., Almar, R., Benveniste, J., and Legeais, J. F.: Altimetry-based sea level trends along the coasts of western Africa, Advances in Space Research, 68, 504–522, 2021.

McLain, D. R.: Heat and water balance of Lynn Canal, Alaska, University of Michigan, 1969.

Melet, A., Almar, R., Hemer, M., Le Cozannet, G., Meyssignac, B., and Ruggiero, P.: Contribution of wave setup to projected coastal sea level changes, J. Geophys. Res. Oceans, 125, e2020JC016078, 2020.

Mercier, F., Picot, N., Lambin, J., Lombard, A., Dibarboure, G., Dufau, C., Carrere, L., Thibaut, P., Obligis, E., and Labroue, S.: Improved Jason-2 altimetry products for coastal zones and continental waters (PISTACH Project), in: AGU Fall Meeting Abstracts, G31B-0662, 2008.

Mohamed, B., Abdallah, A. M., El-Din Khaled Alam and Nagy, H., and Shaltout, M.: Inter-Annual Variability and Trends of Sea Level and Sea Surface Temperature in the Mediterranean Sea over the Last 25 Years, Pure Appl. Geophys., 176, 3787–3810, https://doi.org/10.1007/s00024-019-02156-w, 2019.

Negroni, S., McGillicuddy Jr, D. J., Gawarkiewicz Glen G. and Oddo, P., and Pinardi, N.: Biochemical implications of the Bottom Boundary Layer Detachment at the Mid-Atlantic Bight shelf-break front, Cont. Shelf Res., 286, https://doi.org/10.1016/j.csr.2025.105408, 2025.

Oelsmann, J., Passaro, M., Dettmering, D., Schwatke, C., Sánchez, L., and Seitz, F.: The zone of influence: Matching sea level variability from coastal altimetry and tide gauges for vertical land motion estimation, Ocean Science, 17, 35–57, https://doi.org/10.5194/os-17-35-2021, 2021.

https://doi.org/10.5194/egusphere-2026-4902
Preprint. Discussion started: 27 August 2026

Oelsmann, J., Calafat, F. M., Passaro, M., Hughes, C., Richter, K., Piecuch, C., Wise, A., Katsman, C., Dettmering, D., and Seitz, F.: Coherent modes of global coastal sea level variability, J. Geophys. Res. Oceans, 129, e2024JC021120, 2024.

Paris, P. J., Walsh, J. P., and Corbett, D. R.: Where the continent ends, Geophys. Res. Lett., 43, 12–208, 2016.

Passaro, M., Cipollini, P., Vignudelli, S., Quartly, G. D., and Snaith, H. M.: ALES: A multi-mission adaptive subwaveform retracker for coastal and open ocean altimetry, Remote Sens. Environ., 145, 173–189, https://doi.org/10.1016/j.rse.2014.02.008, 2014.

Passaro, M., Cipollini, P., and Benveniste, J.: Annual sea level variability of the coastal ocean: The Baltic Sea-North Sea transition zone, J. Geophys. Res. Oceans, 120, 3061–3078, https://doi.org/10.1002/2014JC010510, 2015.

Ponte, R. M., Meyssignac, B., Domingues, C. M., Stammer, D., Cazenave, A., and Lopez, T.: Relationships Between Coastal Sea Level and Large Scale Ocean Circulation, Springer, 2020.

Prandi, P., Cazenave, A., and Becker, M.: Is coastal mean sea level rising faster than the global mean? A comparison between tide gauges and satellite altimetry over 1993-2007, Geophys. Res. Lett., 36, https://doi.org/10.1029/2008GL036564, 2009.

Stations with Ellipsoidal Links: https://psmsl.org/data/obtaining/ellipsoidal_links.php, last access: 12 January 2026.

Qin, J., Li, S., Yao, H., Fu, B., He, H., Wang, F., Liu, L., Fan, D., He, X., and Li, Y.: Synergistic multi-altimeter for estimating water level in the coastal zone of Beibu Gulf using SEL, ALES plus and BFAST algorithms, Front. Mar. Sci., 9, https://doi.org/10.3389/fmars.2022.1113387, 2023.

Saucier, F. J. and Chassé, J.: Tidal circulation and buoyancy effects in the St. Lawrence Estuary, Atmosphere - Ocean, 38, 505–556, https://doi.org/10.1080/07055900.2000.9649658, 2000.

Schlembach, F., Ehlers, F., Kleinherenbrink, M., Passaro, M., Dettmering, D., Seitz, F., and Slobbe, C.: Benefits of fully focused SAR altimetry to coastal wave height estimates: A case study in the North Sea, Remote Sens. Environ., 289, https://doi.org/10.1016/j.rse.2023.113517, 2023.

Siedlecki, S. A., Archer, D. E., and Mahadevan, A.: Nutrient exchange and ventilation of benthic gases across the continental shelf break, J. Geophys. Res. Oceans, 116, 2011.

Skov, H. and Durinck, J.: Constancy of frontal aggregations of seabirds at the shelf break in the Skagerrak, J. Sea Res., 39, 305–311, https://doi.org/10.1016/S1385-1101(98)00003-3, 1998.

Swallow, M.: The Sea: ideas and observations on progress in the study of the seas, 1963.

Todd, R. E., Gawarkiewicz, G. G., and Owens, W. B.: Horizontal Scales of Variability over the Middle Atlantic Bight Shelf Break and Continental Rise from Finescale Observations, J. Phys. Oceanogr., 43, 222–230, https://doi.org/10.1175/JPO-D-12-099.1, 2013.

Valladeau, G., Thibaut, P., Picard, B., Poisson, J. C., Tran, N., Picot, N., and Guillot, A.: Using SARAL/AltiKa to improve Ka-band altimeter measurements for coastal zones, hydrology and ice: The PEACHI prototype, Marine Geodesy, 38, 124–142, 2015.

Vignudelli, S., Cipollini, P., Roblou, L., Lyard, F., Gasparini, G. P., Manzella, G., and Astraldi, M.: Improved satellite altimetry in coastal systems: Case study of the Corsica Channel (Mediterranean Sea), Geophys. Res. Lett., 32, 1–5, https://doi.org/10.1029/2005GL022602, 2005.

Vignudelli, S., Cipollini, P., Gommenginger, C., Snaith, H., Coelho, H., Fernandes, J., Gomez-Enri, J., Martin-Puig, C., Woodworth, P., and Dinardo, S.: The COASTALT project: Towards an operational use of satellite altimetry in the coastal zone, in: OCEANS 2009, 1–6, 2009.

Vignudelli, S., Kostianoy, A. G., Cipollini, P., and Benveniste, J.: Coastal altimetry, Springer Science & Business Media, 2011a.

Vignudelli, S., Cipollini, P., Gommenginger, C., Gleason, S., Snaith, H. M., Coelho, H., Fernandes, M. J., Lázaro, C., Nunes, A. L., and Gómez-Enri, J.: Satellite altimetry: sailing closer to the coast, Remote sensing of the changing oceans, 217–238, 2011b.

Vignudelli, S., Birol, F., Benveniste, J., Fu, L.-L., Picot, N., Raynal, M., and Roinard, H.: Satellite Altimetry Measurements of Sea Level in the Coastal Zone, Surv. Geophys., 40, 1319–1349, https://doi.org/10.1007/s10712-019-09569-1, 2019.

Vinogradov, S. V. and Ponte, R. M.: Annual cycle in coastal sea level from tide gauges and altimetry, J. Geophys. Res. Oceans, 115, https://doi.org/10.1029/2009JC005767, 2010.

Vinogradov, S. V. and Ponte, R. M.: Low-frequency variability in coastal sea level from tide gauges and altimetry, J. Geophys. Res. Oceans, 116, https://doi.org/10.1029/2011JC007034, 2011.

Violante-Carvalho, N., Arruda, W. Z., Carvalho, L. M., Rogers, W. E., and Passaro, M.: Diffraction of irregular ocean waves measured by altimeter in the lee of islands, Remote Sens. Environ., 265, 112653, https://doi.org/10.1016/J.RSE.2021.112653, 2021.

Wang, H. and Huang, Z.: Waveform Decontamination for Improving Satellite Radar Altimeter Data Over Nearshore Area: Upgraded Algorithm and Validation, Front. Earth Sci. (Lausanne)., 9, https://doi.org/10.3389/feart.2021.748401, 2021.

Wells, J. T.: Chapter 6 Tide-Dominated Estuaries and Tidal Rivers, in: Geomorphology and Sedimentology of Estuaries, vol. 53, edited by: Perillo, G. M. E., Elsevier, 179–205, https://doi.org/https://doi.org/10.1016/S0070-4571(05)80026-3, 1995.

Wise, A., Calafat, F. M., Hughes, C. W., Jevrejeva, S., Katsman, C. A., Oelsmann, J., Piecuch, C., Polton, J., and Richter, K.: Using shelf-edge transport composition and sensitivity experiments to understand processes driving sea level on the Northwest European shelf, J. Geophys. Res. Oceans, 129, e2023JC020587, 2024.

Woodworth, P. L., Hunter, J. R., Marcos, M., Caldwell, P., Menéndez, M., and Haigh, I.: Towards a global higher-frequency sea level dataset, Geosci. Data J., 3, 50–59, 2016.

Woodworth, P. L., Melet, A., Marcos, M., Ray, R. D., Wöppelmann, G., Sasaki, Y. N., Cirano, M., Hibbert, A., Huthnance, J. M., Monserrat, S., and Merrifield, M. A.: Forcing Factors Affecting Sea Level Changes at the Coast, https://doi.org/10.1007/s10712-019-09531-1, 1 November 2019.

Zhang, J., Guo, X., Zhao, L., Miyazawa, Y., and Sun, Q.: Water Exchange across Isobaths over the Continental Shelf of the East China Sea, J. Phys. Oceanogr., 47, 1043–1060, https://doi.org/10.1175/JPO-D-16-0231.1, 2017.

https://doi.org/10.5194/egusphere-2026-4902
Preprint. Discussion started: 27 August 2026

Zhao, L. and Guo, X.: Influence of cross-shelf water transport on nutrients and phytoplankton in the East China Sea: a model study, Ocean Science, 7, 27–43, 2011a.

Zhao, L. and Guo, X.: Influence of cross-shelf water transport on nutrients and phytoplankton in the East China Sea: a model study, OCEAN SCIENCE, 7, 27–43, https://doi.org/10.5194/os-7-27-2011, 2011b.